NIST Technical Note
NIST TN 2325

The NIST 20 MW Calorimetry Measurement System – Exhaust Flow Characterization and Calibration

Rodney A. Bryant
Artur A. Chernovsky

This publication is available free of charge from:
https://doi.org/10.6028/NIST.TN.2325

NIST NATIONAL INSTITUTE OF STANDARDS AND TECHNOLOGY
U.S. DEPARTMENT OF COMMERCE

NIST Technical Note
NIST TN 2325

The NIST 20 MW Calorimetry Measurement System – Exhaust Flow Characterization and Calibration

Rodney A. Bryant
Artur A. Chernovsky
Fire Research Division
Engineering Laboratory

This publication is available free of charge from:
https://doi.org/10.6028/NIST.TN.2325

January 2025

U.S. Department of Commerce
Gina M. Raimondo, Secretary

National Institute of Standards and Technology
Charles H. Romine, performing the non-exclusive functions and duties of the Under Secretary of Commerce for Standards and Technology and Director, National Institute of Standards and Technology

NIST TN 2325
January 2025

Publication History
Approved by the NIST Editorial Review Board on 2024-12-13

How to Cite this NIST Technical Series Publication
Bryant RA and Chernovsky AA (2025) The NIST 20 MW Calorimetry Measurement System – Exhaust Flow Characterization and Calibration. (National Institute of Standards and Technology, Gaithersburg, MD), NIST Technical Note (TN) NIST TN 2325. https://doi.org/10.6028/NIST.TN.2325

NIST Author ORCID iDs
Rodney A. Bryant: 0000-0002-5344-9878
Artur A. Chernovsky: 0000-0002-1215-7350

.

Abstract

Accurate flow measurements at the exhaust systems of large fire test facilities are critical for achieving accurate measurements of heat release rate. A detailed characterization of exhaust flow for the National Fire Research Laboratory (NFRL) has been conducted to verify the accuracy of its routine flow monitoring devices. Following the procedures of standard test methods for determining average flow in exhaust ducts and stacks, experiments were conducted using S-probes to measure the flow distribution on two orthogonal chords of the exhaust ducts. The results characterize the distribution of near-axial velocity, flow angle, and gas temperature at each of the exhaust ducts, and provide data to evaluate the impact of the fire and off-axis flow on the flow distribution. Routine flow monitoring during large fire experiments in the NFRL is provided by averaging pitot probes installed in the exhaust ducts. Average velocity computed from the flow distributions served as a reference measurement and was used to determine flow calibration constants with estimates of expanded uncertainty ranging from 6 % to 7 %. Agreement with calibration constants determined previously using tracer gas dilution was confirmed, completing the goal of conducting in-line calibrations of NFRL's averaging pitot probes using independent reference measurements to verify measurement accuracy. This effort has established a benchmark for the accuracy of NFRL's exhaust flow measurement and exhaust flow characterization. It has also provided additional evidence that in-situ calibration of the flow monitoring devices used for large fire calorimetry is best practice. Procedures for the flow calibration exist as consensus standards and can be applied for similar large fire test facilities.

Keywords

Flow Characterization; Flow Calibration; S-Probe; S-type Pitot; Large Fire Calorimetry; Emissions; Exhaust Flow Monitoring.

Table of Contents

List of Tables

List of Figures

Acknowledgments

The authors gratefully acknowledge Richard Norcross and Joe Falco of the System Integration Division for engineering support for the automated traverse probes. We are sincerely grateful to Iosif Shinder of the Sensor Science Division for flow calibration services. Research support by the Greenhouse Gas Measurements Program, James Whetstone, Program Manager, NIST Special Programs Office, is also gratefully acknowledged. Finally, we are indebted to technicians Marco Fernandez, Anthony Chakalis, Phillip Deardorff, Laurean DeLauter, and Brian Story, of the Fire Research Division, for their operations and fabrication support.

1. Introduction

Oxygen consumption calorimetry is the most widely used method for measuring the rate of heat release, $\dot{Q}_{\mathrm{OC}}$, during a large fire experiment. Quantitative determination of heat release rate by this method requires complete capture of the fire plume into a flue gas exhaust system and measurement of the amount of oxygen depleted from the exhaust stream (flue gas) by the fire. A simplified measurement model is described by Eq. (1), where $(\Delta_{\mathrm{c}}H_{\mathrm{fuel}})_{\mathrm{O}_2}$ is the heat of combustion per unit mass of oxygen consumed, $\dot{m}_{O_2}^{o}$ is the mass flow of oxygen in the exhaust duct prior to the fire, and $\dot{m}_{O_2}$ is the mass flow of oxygen in the exhaust duct during the fire. The mass flow of oxygen is primarily determined from measurements of the average velocity of the exhaust flow and volume fraction of oxygen in the exhaust stream. [1, 2]

$$\dot{Q}_{\mathrm{OC}} = (\Delta_{\mathrm{c}}H_{\mathrm{fuel}})_{\mathrm{O}_2}\left(\dot{m}_{O_2}^{o} - \dot{m}_{O_2}\right) \qquad (1)$$

Heat release rate (HRR) is the primary measurement for estimating the magnitude of the hazard for a burning item. Therefore, accurate measurements of heat release rate are necessary inputs into models for predicting fire growth and fire spread. However, accurate measurements in large fire calorimeters are difficult due to the challenges associated with making accurate measurements of the exhaust flow. This is often due to under-developed flows or a lack of symmetry of the flow profiles in the large exhaust ducts. Multiple studies have cited the exhaust flow measurement as a significant source of uncertainty when measuring the rate of heat release. [3-8] Consensus standards for open calorimetry fire testing, such as American Society for Testing and Materials (ASTM) E2067, International Organization for Standardization (ISO) 24473, and National Fire Protection Association (NFPA) 286, provide guidance in the form of a heat release rate calibration (overall system calibration) that corrects for the error in the flow measurement. [9-12] However, correcting the flow measurement based on the comparison with heat release rate determined by fuel consumption calorimetry – such as a gas burner – couples any error in determining heat content and fuel flow at the burner with that of the calorimeter.

Conducting an in-situ calibration of the device for measuring exhaust flow is best practice. ASTM E2067 and ISO 24473 recommend, but do not require, an in-situ calibration of the flow measurement device (bi-directional probe or the orifice plate) by conducting a velocity traverse across the exhaust duct to determine the flow distribution. The calibration constant, the ratio of the average velocity determined from the distribution measurement to the centerline (or orifice plate) measurement, becomes the correction for flow measurement. Neither ASTM E2067 nor ISO 24473 provide sufficient detail on conducting the velocity traverse. However, test methods exist for this purpose, as they were developed by the industry for monitoring emissions due to fossil fuel combustion at stationary sources. Test methods, such as Environmental Protection Agency (EPA) Method 2G (40 CFR Part 60), ASTM D3154, and ISO 10780, provide detailed procedures for conducting velocity traverses to determine average velocity in ducts, stacks, or flue pipes. [13-15] These are reference test methods that recommend pitot type probes for in-line calibrations of flow monitoring devices that are part of

a continuous emissions monitoring systems (CEMS). A CEMS consists of integrated instruments permanently installed at a smokestack or flue-gas exhaust system to continuously measure volumetric flow and pollutant concentration. These systems are required to monitor the emissions rate of regulated pollutants and greenhouse gases. Regulatory agencies such as the U.S. Environmental Protection Agency (EPA) require periodic audits of CEMS using consensus standards or test methods as references to evaluate the accuracy of emissions reporting. These standards and test methods can also be applied to improve the accuracy of large fire calorimetry measurements.

Averaging pitot probes (APP) have been installed in the exhaust ducts of the National Fire Research Laboratory (NFRL) to provide continuous measurements of exhaust flow during large fire experiments. The devices are commercially available and widely used to monitor flows for industrial processes. Details of their application in the NFRL have been described in previous publications [1, 16] and will be summarized here. This report will describe the methodology and equipment used to conduct flow traverse measurements using an S-probe. The measurements provide a detailed characterization of the exhaust flow for a system of large fire calorimeters. The flow characterization also provides an in-line calibration of the continuous flow measurement devices, the averaging pitot probes. Results are compared with those of a previously conducted calibration using tracer gas dilution (TGD) as the reference flow measurement. [17, 18]

2. Measurement Methods

Two measurement methods are considered, flow traverse using S-probes and static-mounted averaging pitot probes (APP). Both methods employ impact pressure devices that infer the velocity of a flowing gas or liquid from the measurement of pressure differential across the device induced by the flow. The flow traverse method positions pitot-type probes to gather measurements of flow velocity at discrete points across the exhaust duct. The measurements provide velocity profiles used to estimate the distribution of velocity across the duct, and hence estimate the average exhaust velocity. Flow traverse methods provide detailed characteristics of exhaust flows and are regarded as the standard technique for evaluating the accuracy of routine or continuous flow monitoring devices like averaging pitot probes when applied in the field. A summary of the flow traverse method is described. Averaging pitot probes are utilized to determine average flow velocity along a chord length of an exhaust duct (length of the probe). They have multiple pressure ports spaced along the length of the probe which are integrated to provide a single measurement for estimating average differential pressure. The theory of operation of the averaging pitot probe has been described in a prior publication [16] and will not be repeated here. The reader is encouraged to consult the article for more details. Descriptions of the equipment and experiment procedures utilized in this study are provided in later sections of this document.

2.1. Flow Traverse Method

Procedures for determining the average gas velocity in ducts, stacks, or flues have been established in the following standard test methods – ASTM D3154, EPA Method 1, Method 2, and Method 2G. [13, 14, 19, 20] The procedures specify the use of pitot type probes to measure gas velocity at discrete points. For combustion gases or particulate and droplet laden flows, the “S-probe”, a special pitot probe with large and symmetric openings, is recommended as it is not easily clogged, Fig. 1. The calibration constant for the S-probe, C_{SP}, is assigned a value of 0.84 when its dimensional parameters are compliant with EPA Method 2. [20] However, calibration of the S-probe is recommended for increased accuracy.

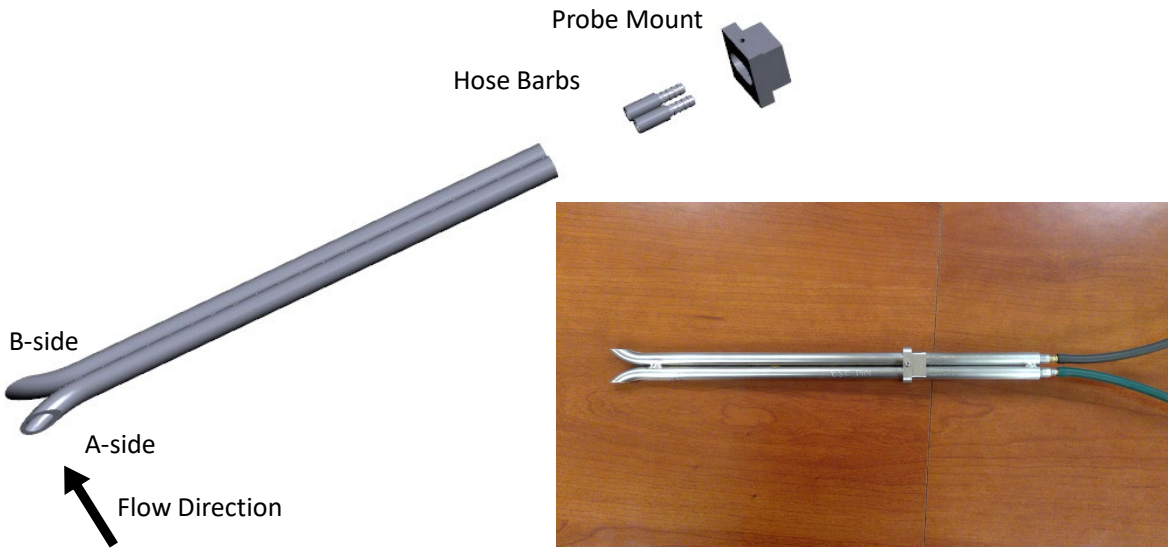

Fig. 1. Exploded-view diagram and photograph of an S-probe.

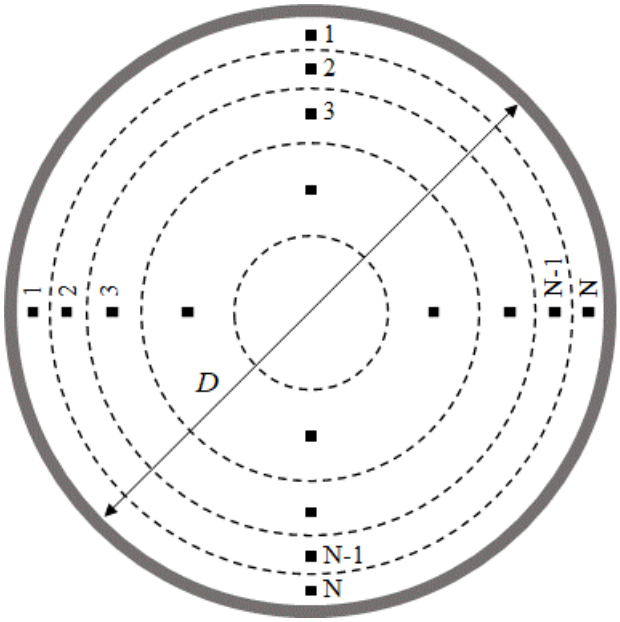

Fig. 2. Traverse positions for centroid of equal areas.

The S-probes are traversed across the duct on a minimum of two chords and velocity is measured at prescribed locations along each chord. Orthogonal chords are selected, as shown in Fig. 2, unless prevented by physical obstructions. The number of measurements locations, N, along a chord depend on the size of the duct and the distance of flow disturbances (bends or

turns) from the measurement site. For circular cross sections, measurements are located at the center of annular regions of equal area (centroid of equal areas - CEA), Fig. 2. The locations for any even number of CEA positions can be computed relative to the chord length, D, using Eq. (2). Table B.1 in Appendix B provides examples of the computed locations. Using CEA positions assigns equal weighting to each measurement; hence the arithmetic average of the measurements represents the average velocity.

$$\frac{d_{\mathrm{i}}}{D} = \frac{1}{2} - \sqrt{\frac{|N-2i+1|}{4N}},\ i = 1, \ldots, \frac{N}{2}$$

$$\frac{d_{\mathrm{i}}}{D} = \frac{1}{2} + \sqrt{\frac{|N-2i+1|}{4N}},\ i = \frac{N}{2}+1, \ldots, N \qquad (2)$$

3. Materials and Procedures

3.1. Flue Gas Exhaust System

The NFRL utilizes large canopy hoods to capture the combustion products generated by the fire experiments. The exhaust hoods are suspended above the test floor and serviced by exhaust ducts that transport the combustion products to an emissions control system (ECS) for conditioning before release into the atmosphere. Each exhaust hood also serves as an oxygen consumption calorimeter, denoted by its fire capacity – 0.5 MW, 3 MW, 10 MW, and 20 MW. Photographs of confirmation experiments using natural gas burners are shown for each calorimeter in Fig. 3. Details of each canopy hood and its associated exhaust path are listed in Table 1. The 0.5 MW calorimeter was not used for this study; therefore, all results will be for the exhaust ducts servicing the larger calorimeters.

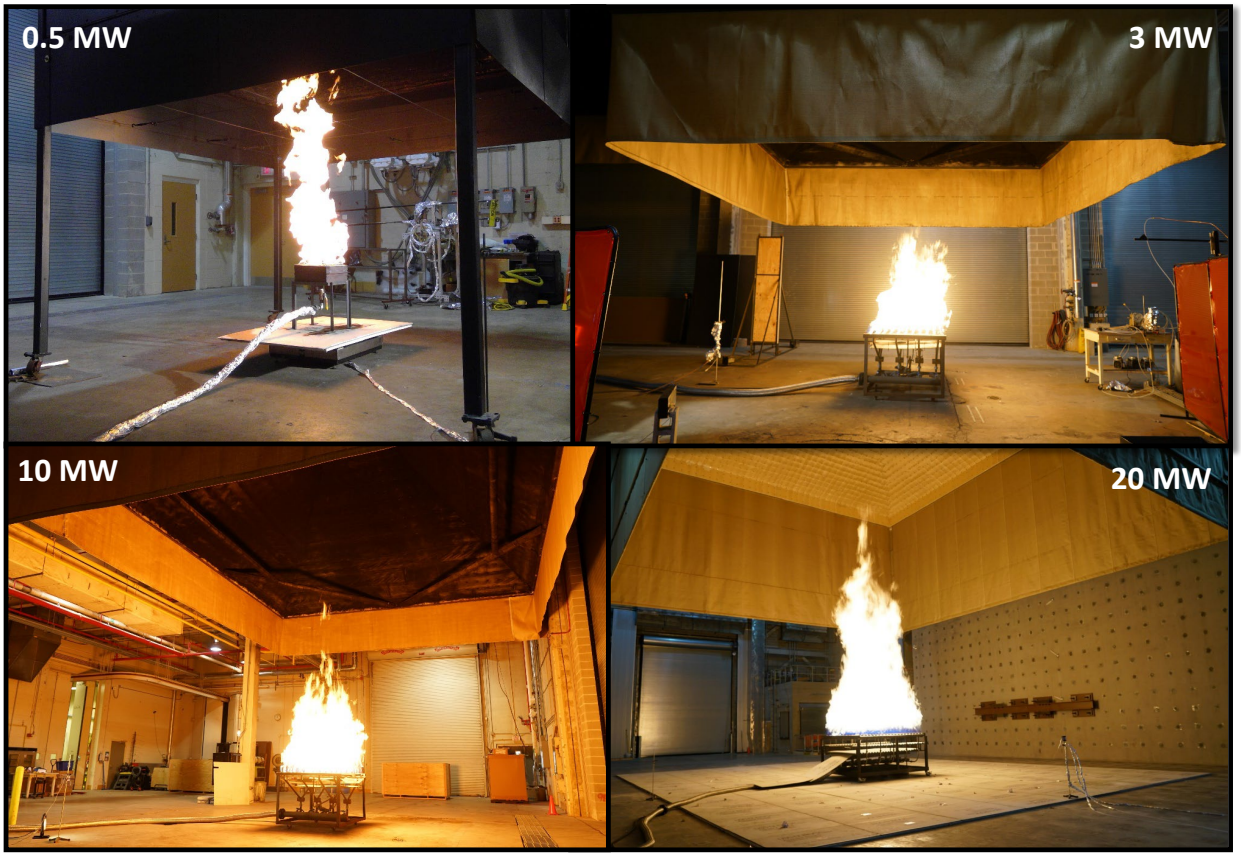

Fig. 3. Canopy hoods and natural gas burners at each of NFRL's calorimeters.

Table 1 Details of the canopy hoods and exhaust system.

Canopy Hood	Duct Inner Diameter	Flow Capacity	Fire Capacity
m x m	m	kg/s	MW
3.1 × 3.2	0.483	4.3	0.5
6.1 × 6.1	1.975	27.5	3
8.4 × 12.4	1.975	58.2	10
13.8 × 15.4	2.424	116	20

The exhaust ducts run along the roof of the facility, as shown in Fig. 4. Instrument measurement stations, NFRL's analog to CEMS, are located upstream of the ECS. Here species volume fraction (concentration), temperature, and velocity of the exhaust gas are monitored and used to determine the emission rates of fire products. The 3 MW and 10 MW calorimeters are serviced by the same exhaust duct (ID 1.975 m), hence the flow at the measurement station is influenced by two possible flow paths. Flow is pulled through the exhaust system by induced draft fans near the end of the system, making the operating pressure in the ducts slightly below atmospheric. The 20 MW calorimetry system has a mass flow capacity of approximately 116 kg/s. Further details of the exhaust system are provided in a report summarizing the NFRL's calorimetry measurement system. [1]

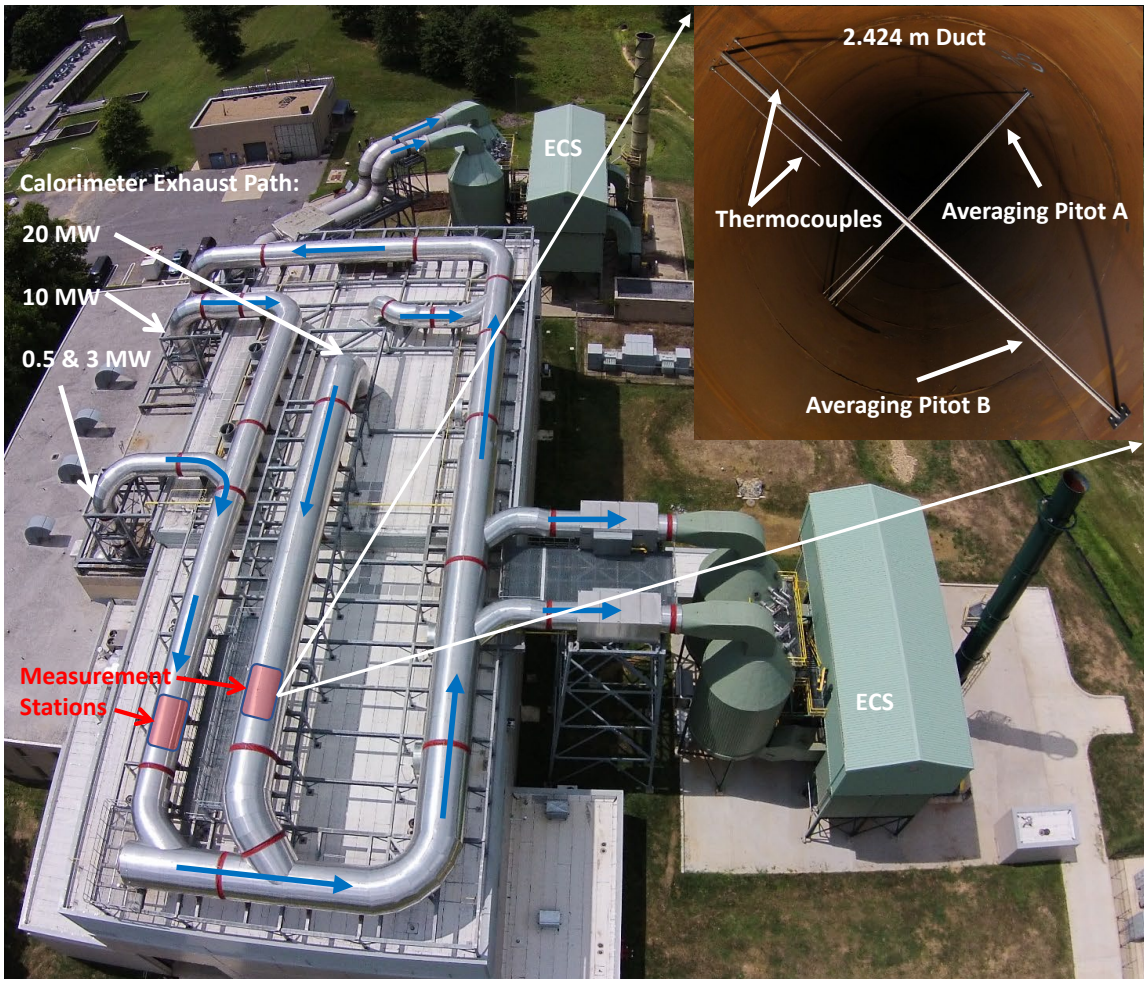

Fig. 4. NFRL's flue gas exhaust system and flow monitoring devices (inset photo).

3.2. Exhaust Flow Measurement – Averaging Pitot Probe

Two (A and B) averaging pitot probes (Rosemont 485 Annubar)[1] are installed at the measurement stations shown in Fig. 4. They monitor gas velocity in each exhaust duct, V_{APP}, as defined by Eq. (3), where $V_{\mathrm{e,A}}$ and $V_{\mathrm{e,B}}$ are measured gas velocity at the respective probe. The averaging pitot probes are NFRL's routine (or continuous) flow measurement devices, analogous to a CEMS flow measurement at a stationary source. Estimates of gas temperature are provided by two bare bead thermocouples (Type K) installed adjacent to each probe, T_{APP}.

$$V_{\mathrm{APP}} = \frac{V_{\mathrm{e,A}} + V_{\mathrm{e,B}}}{2} \qquad (3)$$

Theory of operation and technical details of the averaging pitot probes have been described in previous publications summarizing NFRL's flow measurement method [16] and initial in-line

[1] Certain equipment, instruments, software, or materials, commercial or non-commercial, are identified in this document in order to specify the experimental procedure adequately. Such identification does not imply recommendation or endorsement of any product or service by NIST, nor does it imply that the materials or equipment identified are necessarily the best available for the purpose.

calibration experiments for the probes. [17, 18] The reader should consult these documents for additional details.

3.3. Exhaust Flow Measurement – Flow Traverse

The flow distribution in the exhaust duct was measured using an S-probe and bare-bead thermocouple mounted to two traverse probe modules, j = 1, 2. The traverse modules are automated and were used to position the S-probes across the exhaust ducts, measuring the distribution of near axial velocity, $V_{\mathrm{SP,j}}(d)$, at the horizontal (j = 1) and vertical (j = 2) chords. Measurements were conducted at 28 CEA traverse positions on each chord. Additional measurements were conducted at the near wall and the chord center resulting in 33 or more measurements (i = 1, 2, 3, …., 33).

$$V_{\mathrm{SP,j}}(d_i) = C_{\mathrm{SP,j}} \cos\left(\theta(d_i)\right) \sqrt{2\Delta P(d_i) T(d_i) \frac{R}{P_s M_e}} \qquad (4)$$

The S-probes (Environmental Supply Co., PPS12-Y-024) are made from 0.95 cm (3/8 in) stainless steel tubing and fabricated to the specifications defined in EPA Method 2. [20] The bare-bead thermocouple (Omega Type K, 1.00 ± 0.03[2] mm bead diam) was mounted approximately 2.5 cm from the tip of the pressure openings of the S-probe using fiberglass tape. Two precision capacitance manometers (MKS 220D Baratron) were attached to the leads of each S-probe to measure the flow induced pressure differential. The pressure range of the manometers was 0 Pa to 133.32 Pa, for lower speed flows, and 0 Pa to 1333.2 Pa, for higher speed flows. Both were calibrated against NFRL's working standard for pressure (NFRL WSTD 577967), a high-accuracy capacitance manometer (MKS 698A Baratron). The relative expanded uncertainty of the differential pressure measurement is estimated at 1.0 % for the low range transducers (133.32 Pa) and 0.6 % for the high range transducers (1333.2 Pa). The flexible pressure leads were fed through the hollow probe rail to connect the S-probe to the transducers. Wiring for the thermocouple also passed through the probe rail. A photograph of the traverse modules with each S-probe and thermocouple attached to the linear rail is shown in Fig. 5.

Density of the exhaust gas, ρ_e, is derived from the temperature measurement, *T*, at each probe's thermocouple. The relative expanded uncertainty of the gas temperature measurement is estimated at 1.0 % of the absolute temperature reading (K). Static pressure in the exhaust duct, P_s, is measured with a digital barometer (Vaisala PTU303) with an expanded uncertainty of 15 Pa. The molecular mass, M_e, of the exhaust gas is assumed to be equal to that of dry ambient air, (28.97 ± 0.10) kg/kmol.

[2] Unless otherwise stated, all uncertainty values are reported as expanded uncertainty for a 95 % confidence interval (with *k* = 2.0).

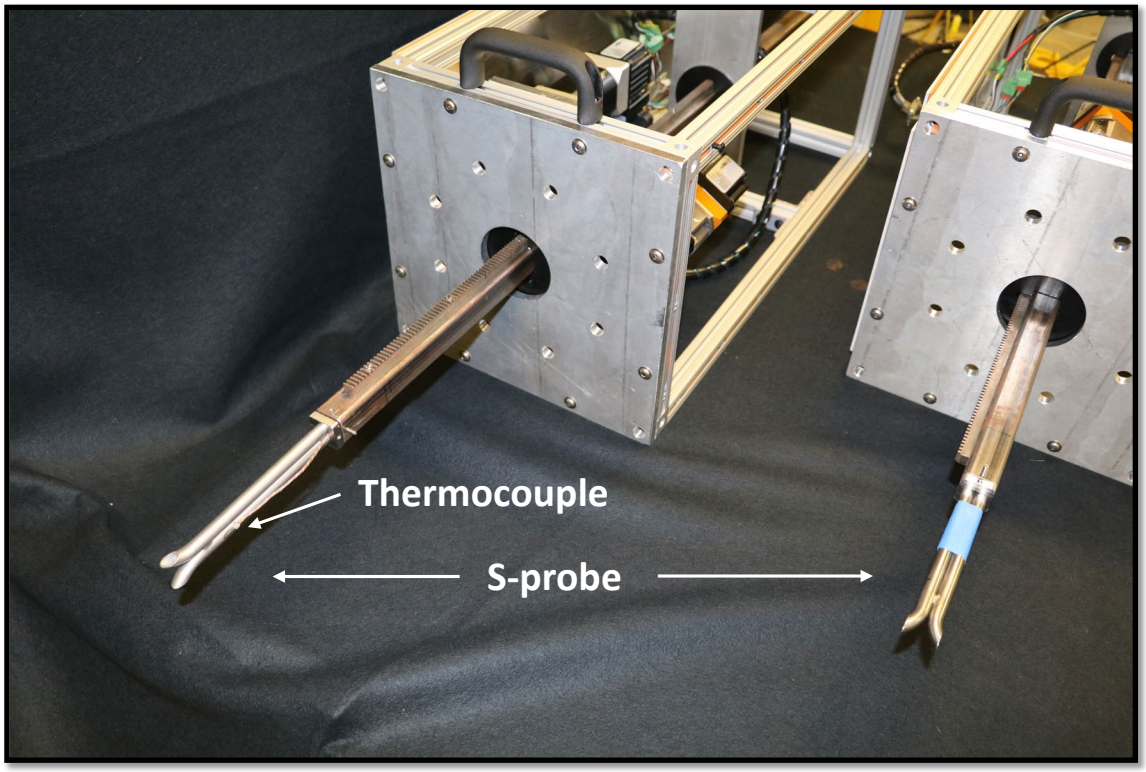

Fig. 5. Photograph of automated traverse modules used for flow traverse experiments. S-probe/thermocouple assembly is attached to each module.

Flow angle, θ, was determined by nulling the S-probe, therefore rotating the probe about its axis until the differential pressure reads zero (null). A linear interpolation of the data in real-time determined the null angle, θ_{null}. Once the null angle was computed the probe rotated 90° in the opposite direction to align it with the flow. Hence the flow angle is $\theta = \theta_{\text{null}} - 90°$ for a clockwise rotation as shown in Fig. 6. Rotational position of the S-probe was measured by a linear encoder at the smartmotor used to position the probe. The expanded uncertainty of the flow angle measurement is estimated at ±3.2°. This estimate is consistent with the range of flow angles measured at any one traverse location (see Fig. 9). Development of the procedure to determine flow angle and the analysis of its uncertainty have been described in a prior report. [21]

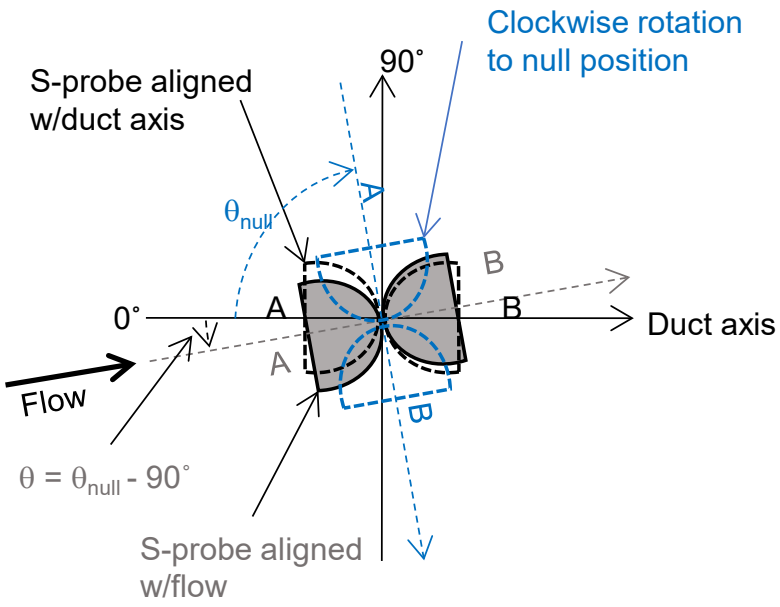

Fig. 6. S-probe orientation during the nulling procedure.

Each S-probe was calibrated in the NIST Airspeed Calibration Facility [22] to determine its calibration coefficient, C_{SP}. Calibrations were performed using the tertiary working standard – a pitot tube, traceable to the International System of units (SI). The relative expanded uncertainty of the working standard is estimated at 0.44 %. [23] Power law fits, listed in Table 2, were derived from the calibration data. They are used to compute the calibration coefficients for each probe as a function of differential pressure. Assuming all directional flow is limited to the plane perpendicular to the rotational axis of the S-Probe, as shown in Fig. 6, the expanded uncertainty of the calibration coefficients for the S-probes used in this study is estimated at ±2.6 %. [21] Without adequate flow conditioning this assumption may not hold. In practice, exhaust flows are 3-dimensional; therefore, the S-probe can be subject to flow from any direction. The calibration data shows the S-probe coefficient to be sensitive to flow direction. Hence, the best accuracy is achieved when the S-probe faces the primary direction of flow. In this study, rotational alignment of the S-probe is limited to a single plane. In the core region of the exhaust duct, the results show the primary flow direction to lie in the plane of rotation of each S-probe. Measured flow angles in the core region are within ±5°, suggesting that the direction of out-of-plane flow is on the same order. Therefore, the expanded uncertainty estimate for the probe coefficients is increased to ±5.2 % based on calibration data for S-probe misalignment within ±5°.

Table 2. Functions for computing S-Probe calibration coefficients with respect to the differential pressure (Pa) at the probe.

	$^{*}C_{SP}$
Probe 1	$0.8036\Delta P^{0.006576}$
Probe 2	$0.7995\Delta P^{0.008514}$

*Valid only for ΔP in units of Pa.

A system of automated traverse probes was designed and fabricated to perform the flow mapping experiments. [21] Two automated probes were mounted to the exhaust ducts on horizontal (j = 1) and vertical (j = 2) chords, as shown in Fig. 7. The probes were mounted upstream of the averaging pitot probes at a distance greater than one duct diameter. Each probe module is remotely operated and fully programmable to traverse the duct, as prescribed by the standard test methods (EPA Methods 1, 2, 2G, ASTM D3154, ISO 10780), and measure the flow distribution across the duct chord. Smartmotors (MOOG Animatics, Model SM23165DT) are utilized to provide precise linear (d) and rotational (θ) positioning of the S-probes in the duct.

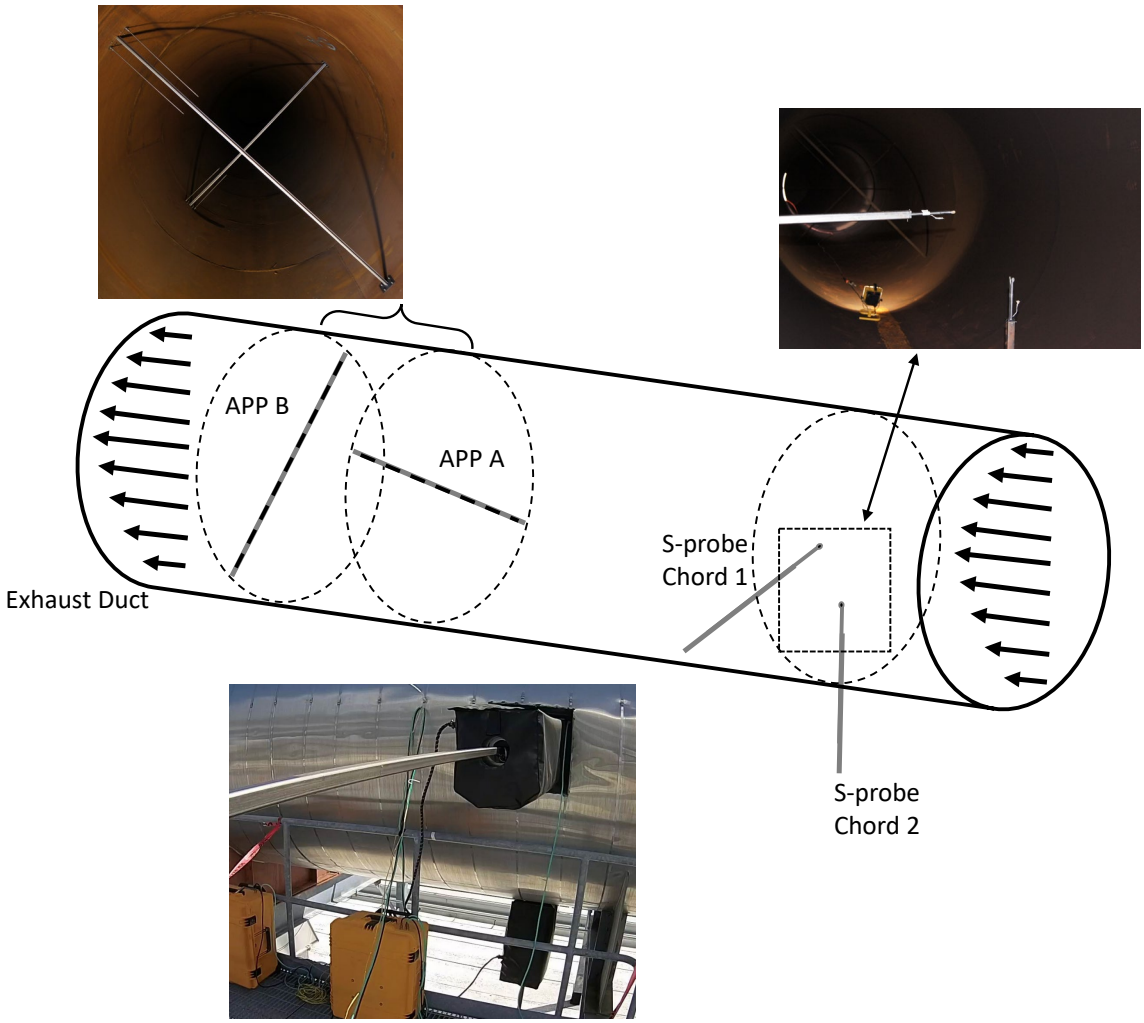

Fig. 7. Diagram of automated traverse modules and averaging pitot probes installed at an exhaust duct at the NFRL. The automated traverse modules are mounted upstream of the averaging pitot probes for simultaneous flow measurements.

3.4. Experimental Procedure

Simultaneous measurements of flow velocity in the exhaust ducts were conducted using the averaging pitot probes (NFRL's flow CEMS) and the S-probe automated traverse system. A typical experiment targeted 3 to 4 flow conditions, with flow measurements traversing a minimum of 28 CEA locations, plus the midpoint and locations at the near wall. Automation of the traverse procedure was accomplished using scripted instructions for probe movement, which were loaded to the automated traverse system. A minimum of 6 repeat experiments were conducted at each flow setpoint. Therefore, the calibration data for each calorimeter consists of a minimum of 24 measurements. The following steps summarize a typical experiment:

1) The exhaust system was initiated, and flow was adjusted to the first target value by monitoring readings from the averaging pitot probes.
2) Each S-probe was positioned at its starting position – 25 mm from the near wall for the probe on the horizontal chord (S-probe 1) and 25 mm from the far wall for the probe on the vertical chord (S-probe 2).
3) The probe traverse began with S-probe 1 moving forward, while S-probe 2 moved in reverse. Each probe paused at the predetermined positions (d_i) to record measurements of flow and flow angle (some experiments were conducted with the probes aligned with the duct axis, $\theta(d_\mathrm{i}) = 0°$).
4) Flow readings from the averaging pitot probes ($\Delta P_{\mathrm{APP,i}}$, $T_{\mathrm{APP,i}}$) and S-probes (d_i, $\Delta P(d_\mathrm{i})$, $T(d_\mathrm{i})$, $\theta(d_\mathrm{i})$, $P_{\mathrm{s,i}}$) were continuously logged using NFRL's data acquisition system. Measurements at the predetermined positions were tagged for later analysis.
5) After the flow traverse was completed, the exhaust flow was adjusted to a new target value. The S-probes were moved to their starting positions, and the next probe traverse initiated.

Probe positioning was scheduled in the scripts to avoid probe collisions or measurement interference. Nulling the probes to determine flow angle added significant time to the experiments. Preliminary analysis revealed that on average, flow angle was within ±5°. Examining Eq. (4), it is predicted that such small flow angles should have a negligible impact on the average flow estimate. Therefore, many experiments were conducted with the S-probes aligned with the axis of the duct, $\theta(d_\mathrm{i}) = 0°$, to generate data to confirm the prediction.

Ideally the flow traverse would be conducted with a fire present to create a heated flow and characterize its impact on the flow. A traverse experiment requires more than 30 minutes to complete. It is not prudent to have a fire present for each experiment, therefore it was an added condition for a limited number of experiments. NFRL's natural gas burners were used to simulate fire conditions (see Fig. 3) and thus generate enough data to characterize the impact of a fire.

4. Results and Discussion

4.1. Flow Characterization

Data for the exhaust flow at the 3 MW, 10 MW, and 20 MW calorimeters are summarized in Fig. 8, showing the flow distribution at the horizontal (1) and vertical (2) chords. Normalizing the velocity measurements from the traverse probes with the flow velocity determined at the averaging pitot probes collapsed the data from four target flows into a single distribution for each chord. Using a linear regression analysis with the least squares approach, a six-degree polynomial was chosen to fit the collapsed data. The distribution ranged from 70 % to 125 % of the flow speed monitored by the averaging pitot probes. Data from experiments for which the natural gas fire was added to generate a heated flow is included. Measurements with ($\theta = \theta_{\text{null}} \pm 90°$) and without ($\theta = 0°$) the correction for flow angle as defined in Eq. (4), are also included. The data presented is the result of repeat experiments over a period of 24 months, thus demonstrating the stability of the flow distribution across a range of operating conditions. Data for the flow conditions are presented in Appendix D. Flow velocity at any position along a chord can be estimated using the polynomial fits presented in Appendix E.

Flow distribution measurements at the exhaust duct of the 3 MW calorimeter show that flow is skewed on the horizontal and vertical chords. Peak flow occurs on the near side (200 mm ≤ d ≤ 500 mm) of the duct for the horizontal chord. Flow speeds are approximately 20 % to 30 % greater than flow speeds at opposite locations on the far side (1475 mm ≤ d ≤ 1775 mm). Peak flow occurs on the far side of the duct for the vertical chord, but the side-to-side difference is less, approximately 5 % to 10 %. The results demonstrate clear evidence of skewed flow distributions and is consistent with previous evidence suggesting skewed flow due to an approximately 5 % difference in measurements at averaging pitot probes A and B. [16] Skewed flow distributions can lead to errors in exhaust flow estimates when the flow field is not adequately characterized, such as the practical case of using a single stationary pitot measurement to represent average flow.

Greater flow symmetry was observed at the 10 MW calorimeter, with peak flow occurring close to the center of the duct. This is consistent with data from the averaging pitot probes that show good agreement between the averaging pitot probes A and B. [16] Note that the 3 MW and 10 MW calorimeters share their flow measurement station, Fig. 4, but generate different flow distributions. This is due to the difference in flow path for the two calorimeters. There is a greater number of turns in the flow path for the 3 MW calorimeter, while the 10 MW calorimeter has a much longer section for straight flow.

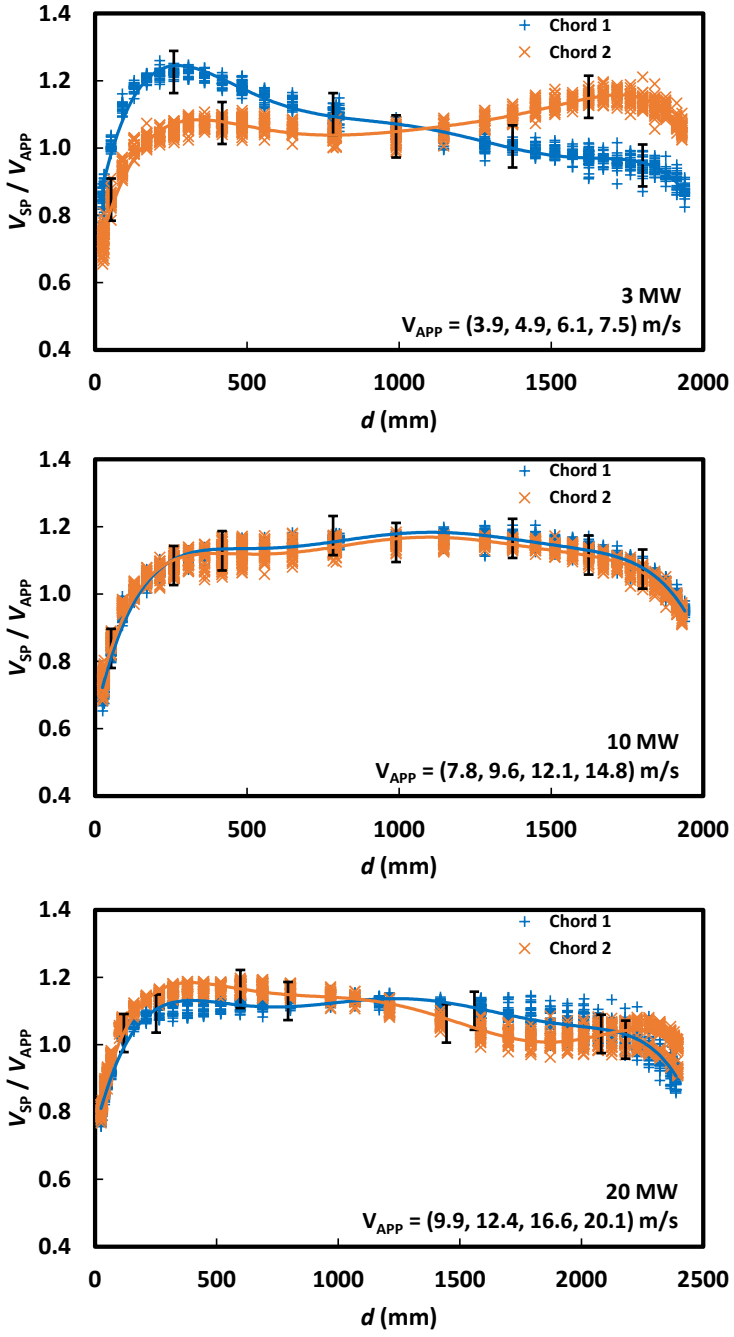

Fig. 8. Relative flow distribution across the exhaust ducts of the 3 MW, 10 MW, and 20 MW calorimeters. Traverses were at the horizontal (1) and vertical (2) chords. Velocity measurements from the S-probes, V_{SP}, are normalized by the corresponding flow monitored at the averaging pitot probes, V_{APP}. Error bars represent estimates of expanded uncertainty. Average flow speed settings are listed for each calorimeter.

The 20 MW calorimeter uses a much larger exhaust duct, 2.4 m, and provides twice the flow capacity of the 10 MW calorimeter. Flow symmetry was observed on the horizontal chord, with peak flow near the center. A slightly skewed distribution was observed on the vertical chord, with peak flow on the near side of the duct. The measurements suggest the overall distribution of flow has symmetry across the vertical axis. This is consistent with evidence from averaging pitot probes A and B as described in a previous study where the ratio of their response is approximately unity, suggesting flow symmetry. [16]

Distributions of flow angle for exhaust flow at the 3 MW, 10 MW, and 20 MW calorimeters are summarized in Fig. 9. The figure includes data from all experiments that measured flow angle to estimate the near axial velocity, Eq. (4). A fifth-degree polynomial was chosen to fit the flow angle data. Flow angle did not exceed ±20° and was within ±5° on average. The exception is at the walls of the duct. As much as 15° of off-axis flow was observed at the far wall of the duct for the 20 MW calorimeter. Flow angles exceeding ±5° were also observed at the near wall of each duct. The mounting ports for the traverse probes are at the near walls of the duct and leakage of flow into the duct at the ports impact the angle of the flow. There is a wider distribution of flow angle near the ports, ranging from negative to positive values. This suggest the flow direction near the port is impacted more by local flow contributions due to leakage instead of the overall evolution of flow. Examining the inner region of the exhaust duct – i.e. away from the walls - the range of the measured flow angle is about 5° ($\theta(d_\mathrm{i}) \pm 2.5°$) at any given location. This suggests a very repeatable measurement when one considers that experiments were conducted over a two-year period and at various conditions. The repeatability is consistent with the estimated uncertainty of the flow angle measurement. Note that the results for flow angle are specific to this exhaust flow configuration. The uncertainty of flow angle measurements may be higher in other field applications, such a stack flows with greater flow swirl.

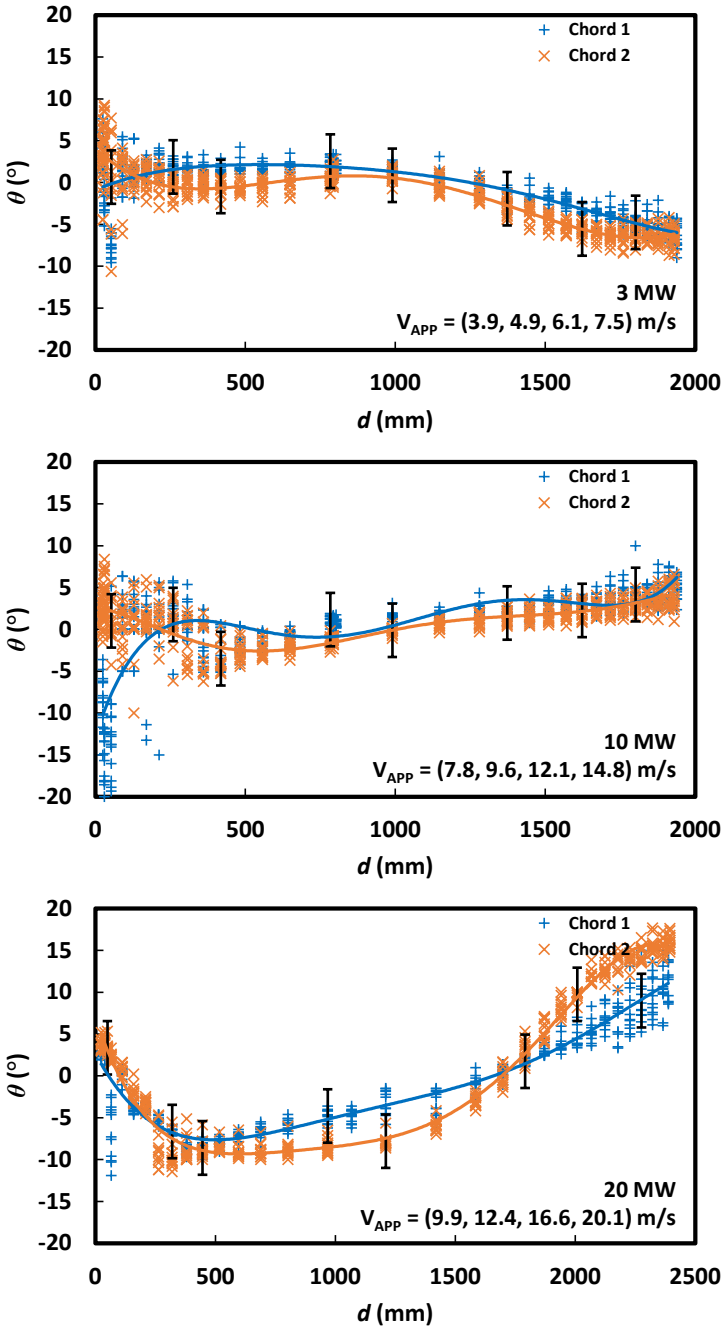

Fig. 9. Distribution of flow angle across the exhaust ducts at the 3 MW, 10 MW, and 20 MW calorimeters. Traverses were at the horizontal (1) and vertical (2) chords. Error bars represent estimates of expanded uncertainty. Average flow speed settings are listed for each calorimeter.

Profiles of relative flow speed for S-probes aligned with off-axis flow ($\theta(d_\mathrm{i}) = \theta_\mathrm{null}(d_\mathrm{i}) \pm 90°$), S-probes aligned with the duct axis ($\theta(d_\mathrm{i}) = 0$), and both cases combined (All Data) are shown in Fig. 10. Flow profiles computed from the least squares regression of the data are plotted for clarity. The error bars represent estimates of relative expanded uncertainty for the velocity traverse measurements, $U_{V_\mathrm{SP}}/V_\mathrm{APP}$. Estimated relative expanded uncertainty is 0.06 on average. Details of the uncertainty estimates are presented in Appendix C. At the 3 MW and 10 MW calorimeters the magnitude of the flow angle is less than 5° on average. An examination of Fig. 10 shows negligible impact on the flow distribution for small flow angles. However, at the 20 MW calorimeter, the magnitude of flow angle is greater than 5° on average. The impact of larger flow angles on the flow distribution is apparent at the walls and on the vertical chord (chord 2) where flow angles approaching 15° were observed.

Due to the extended duration of a traverse experiment, most experiments were conducted using the ambient air as the exhaust flow. For a limited number of experiments, NFRL's natural gas burners were used to simulate fire conditions and thus generate a heated exhaust to characterize the impact of the fire on the flow. At the 3 MW calorimeter four experiments were run using steady fires at 1 MW and 2 MW, Table 3. An examination of Fig. 11, suggests the addition of the fire (heating) had negligible impact on the flow distribution at the 3 MW calorimeter. Four similar experiments were run at the 10 MW calorimeter and the results again demonstrate that the fire had negligible impact. The results at the 20 MW calorimeter suggest the addition of a fire may impact the flow. At the far wall on the horizontal chord (Chord 1), the flow speed increased by as much a 10 %. Due to scheduling, only a single fire experiment could be run. More repeat data will be required to conduct a qualitative evaluation of the impact of fire to the flow at the 20 MW calorimeter. A quantitative evaluation of the impact of off-axis flow and added fire is presented later in Table 5.

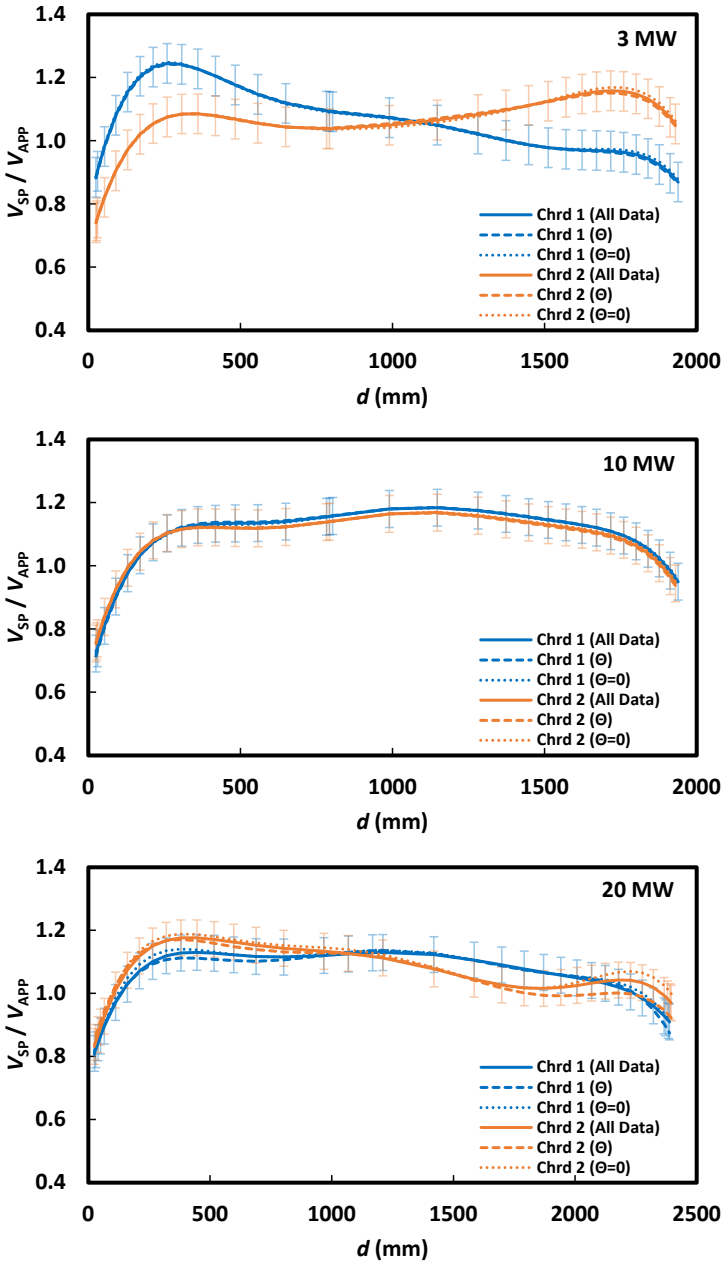

Fig. 10. Comparison to evaluate the impact of flow angle on the flow distribution measurement at the 3 MW, 10 MW, and 20 MW calorimeters. Experiments with flow angle measurement (θ, dashed line), without flow angle measurement (θ=0, dotted line), and all experiments combined (solid line). Error bars represent estimates of expanded uncertainty. Chrd1: Horizontal, Chrd2: Vertical.

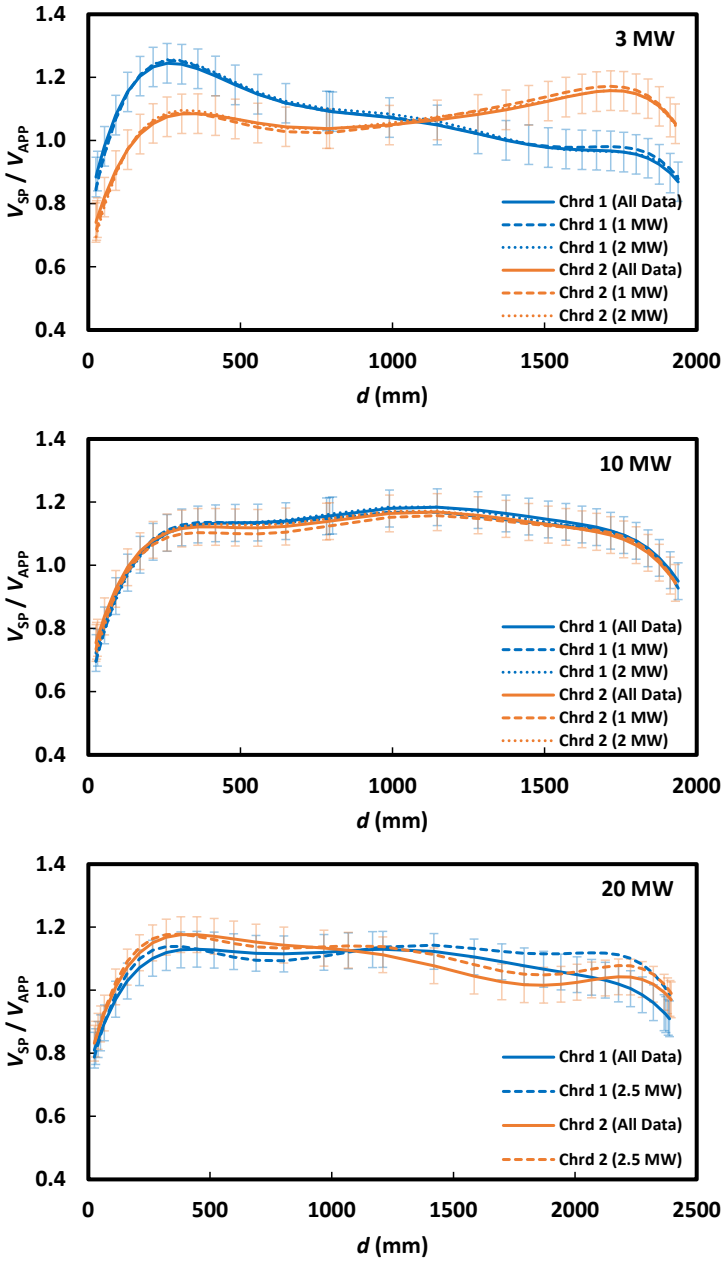

Fig. 11. Comparison to evaluate the impact of a steady fire on exhaust flow distribution at the 3 MW, 10 MW, and 20 MW calorimeters. Experiments with fire (dashed line) and all experiments combined (solid line). Error bars represent estimates of expanded uncertainty. Chrd1: Horizontal, Chrd2: Vertical.

Since each S-probe is equipped with a thermocouple, experiments with simulated fire conditions provide information on the temperature distribution across the exhaust ducts. Thermocouples are also installed at the averaging pitot probes, which are static installations and therefore provide a reference. Table 3 lists the temperatures monitored at the averaging pitot probes during each steady fire experiment. Exhaust gas temperature depends on the amount excess air pulled into the calorimeter for a given fire size. At the 3 MW and 10 MW calorimeters the range of exhaust gas temperature was approximately 30 °C to 100 °C for 1 MW to 2 MW fires. At the 20 MW calorimeter the exhaust gas temperature was approximately 50 °C to 60 °C for a 2.6 MW fire.

Temperature measurements from the S-probes (°C) are normalized by the temperature measured at the averaging pitot probes (°C), providing a relative distribution of exhaust flow temperature at each chord, Fig. 12. Temperature measurements for all fire conditions considered in this study are presented. For distances greater than 100 mm the data show a uniform distribution of temperature across the measurement section. Recall the mounting ports for the traverse probes are at the near walls of the duct and air leakage from the cooler ambient environment causes lower temperatures at the near walls. Ignoring the reduced temperatures due to air leakage, the gas temperature across the exhaust duct deviates from that measured at the averaging pitot probe by less than 3 % in the 3 MW and 10 MW calorimeters. The deviation is less than 5 % at the 20 MW calorimeter, but noting this is for a single experiment. The characterization of flow temperature for the present study demonstrates that the temperature measurement at the averaging pitot probes provides an adequate representation of the distribution of gas temperature across the exhaust duct.

Table 3 Monitored flow speed and flow temperature during steady fire experiments.

Calorimeter	Fire Size (MW)	Monitored Flow Speed V_{APP} (m/s)	Monitored Flow Temperature T_{APP} (°C)
3 MW	1.1	4.5	75.8
3 MW	1.1	5.3	68.0
3 MW	2.1	6.7	98.8
3 MW	1.9	8.2	79.5
10 MW	1.1	8.3	46.3
10 MW	2.0	10.1	58.8
10 MW	2.0	12.7	48.7
10 MW	1.1	14.2	30.7
20 MW	2.6	17.3	54.2

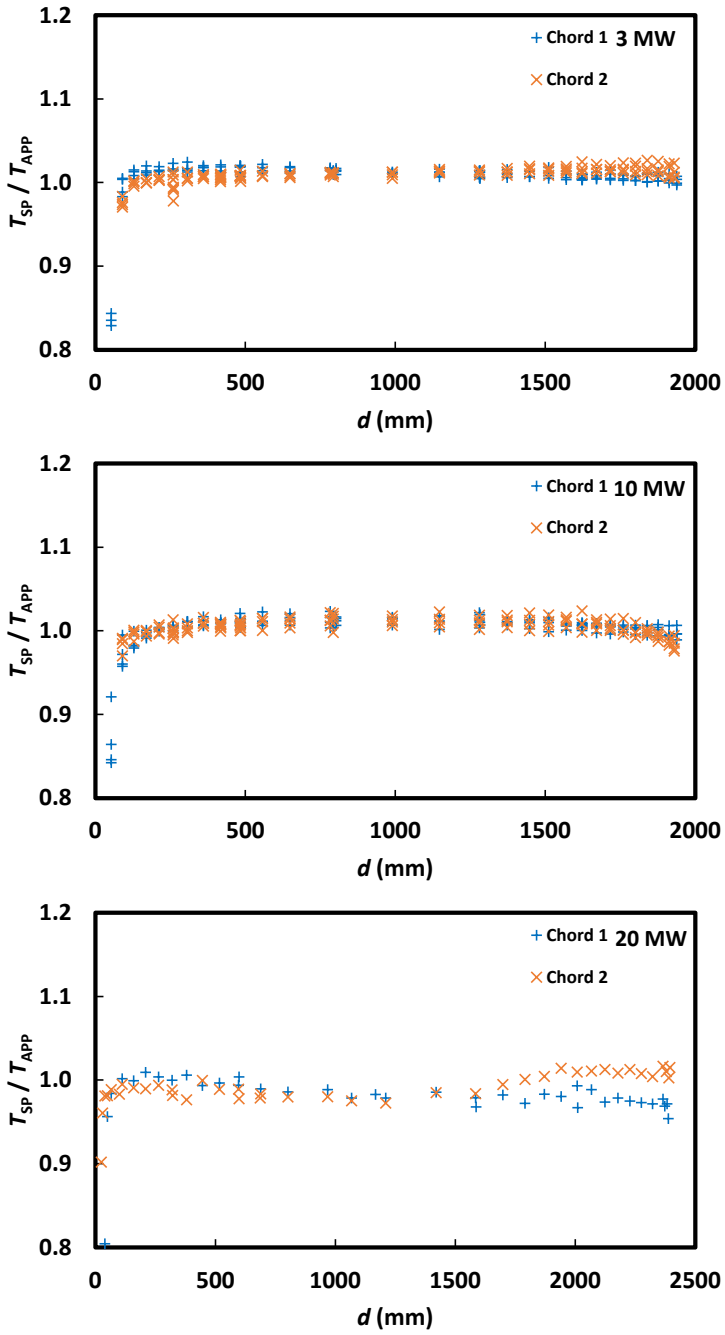

Fig. 12. Relative distribution of gas temperature (°C/°C) across the exhaust ducts at the 3 MW, 10 MW, and 20 MW calorimeters, during experiments with a steady fire. Temperature measurements at the S-probes are normalized by the corresponding temperature measurements at the averaging pitot probes, see Table 3. Chord1: Horizontal, Chord2: Vertical.

4.2. In-Line Calibration of Averaging Pitot Probes

The flow characterization described in the previous section serves as an in-line calibration of the averaging pitot probes. Experiments consisted of 3 to 4 flow settings that targeted approximately 50 %, 60 %, 80 %, and 100 % of mass flow capacity at each calorimeter. At each flow setting, the S-probes were traversed through 28 CEA locations plus additional locations at the near wall and the duct center. For in-line calibrations of exhaust or stack flows, the maximum number of traverse locations on a chord, listed by both EPA and ASTM is 24 (N ≤ 24). [14, 19] The additional traverse locations provide adequate data for interpolating data at 24 CEA locations as shown in Fig. 13. Using the interpolated data, an average velocity ratio was computed for the 24 CEA locations at each experiment, Eq. (5). Average velocity computed from 24 or fewer CEA locations is consistent with the standard test methods (EPA Method 1, EPA Method 2, EPA Method 2G, and ASTM D3154). [13, 14, 19, 20]

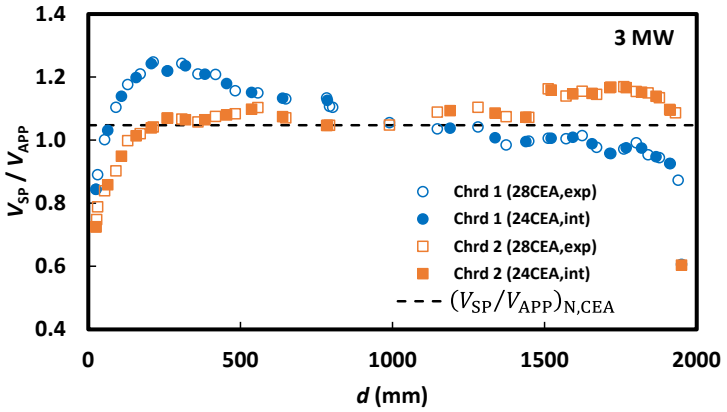

Fig. 13. Interpolated flow distribution (solid symbols) derived from measurements (open symbols). Dashed line represents the average flow ratio, Eq. (5). Chrd1: Horizontal, Chrd2: Vertical.

$$\left(\frac{V_{SP}}{V_{APP}}\right)_{N,CEA} = \frac{1}{2N}\left[\sum\left(\frac{V_{SP,1}}{V_{APP}}(d_i)\right) + \sum\left(\frac{V_{SP,2}}{V_{APP}}(d_i)\right)\right] \qquad (5)$$

The result of Eq. (5) is an average velocity ratio for each experiment as displayed in Fig. 14. A minimum of 6 repeat experiments were conducted at each flow setpoint, resulting in at least 24 calibration measurements ($M \geq 24$) at each calorimeter. Fig. 14 shows the average velocity ratio at each calorimeter as constant across the flow range. Therefore, the calibration constant, C_f, for the exhaust flow measurement is computed as the mean of the ratios, Eq. (6).

$$C_f = \frac{1}{M}\sum\left(\frac{V_{SP}}{V_{APP}}\right)_{N,CEA} \qquad (6)$$

The results show that the flow measurement at the averaging pitot probes under-estimates the average flow velocity determined by the S-probe traverse by 4 % to 5 % on average. This is consistent with previous flow calibration results and measurement comparisons of heat release rate for NFRL's calorimeters. [16-18]

Uncertainty estimates for the flow calibration constants are listed in Table 4. The uncertainty is propagated from estimates of standard uncertainty for the velocity measurements from the S-probe traverses ($\frac{u_{V_{\mathrm{SP}}}}{V_{\mathrm{APP}}}$), the standard deviation of the sample mean for the centroid of equal area method ($\frac{\sigma_{N,CEA}}{\sqrt{2N}}$), and the standard deviation of the sample mean ($\frac{\sigma_{C_{\mathrm{f}}}}{\sqrt{M}}$) of the repeat experiments. The expanded uncertainty, $U_{C_{\mathrm{f}}}$ computed as the square root of the sum of squares of the standard uncertainties and multiplied by the coverage factor, k = 2 for a 95 % confidence interval, ranges from 0.065 to 0.075 with respect to the calorimeter.

Table 4 Uncertainty estimates for the flow calibration constant.

Calorimeter	$\frac{u_{V_{\mathrm{SP}}}}{V_{\mathrm{APP}}}$	$\frac{\sigma_{N,CEA}}{\sqrt{2N}}$	$\frac{\sigma_{C_{\mathrm{f}}}}{\sqrt{M}}$	$U_{C_{\mathrm{f}}}$
3 MW	0.031	0.020	0.001	0.075
10 MW	0.029	0.020	0.001	0.071
20 MW	0.028	0.016	0.002	0.065

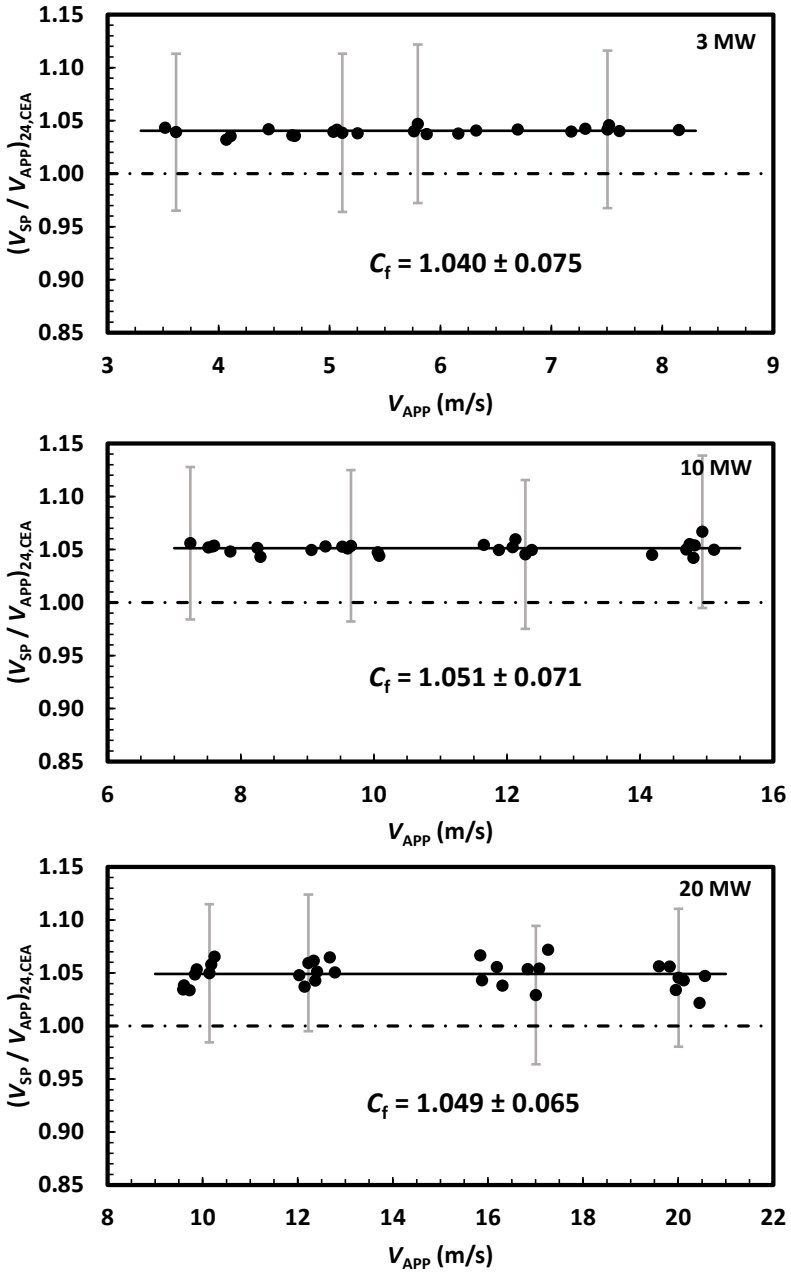

Fig. 14. Results of flow calibration experiments at the 3 MW, 10 MW, and 20 MW calorimeters. The solid line represents the flow calibration constant determined over the range of flow. Error bars represent expanded uncertainty for each velocity ratio.

Flow calibration constants determined from the present flow traverse experiments are listed for each calorimeter in Table 5. They were determined for experiments with and without flow alignment of the S-probes, and for experiments with and without a fire. At the 3 MW and 10 MW calorimeters, flow angles were less than 5° on average. The result is a difference of less than 0.5 % between flow calibration constants determined from measurements for flow-aligned probes and axis-aligned probes. This is consistent with Eq. (4) and EPA's recommendation to align the S-probes with the duct axis whenever the average of absolute flow angle is less than 20°. [19] EPA's recommendation allows for a simpler and faster measurement that still achieves acceptable accuracy. At the 20 MW calorimeter, flow angles approaching 15° were observed. The resulting difference for flow-aligned and axis-aligned calibration constants is approximately 2.0 %, but still within the expanded uncertainty. The addition of natural gas fires at the 3 MW and 10 MW calorimeters changed the flow calibration constant by less the 0.6 %. However, at the 20 MW calorimeter, the addition of the natural gas fire caused the flow calibration constant to increase by 2.2 %. This result is not conclusive as it is inferred from a single experiment with fire. More data is necessary. In all cases, any changes in the calibration constants due to off-axis flow or added fire were less than the estimated uncertainty, Table 4. Hence the calibration constants were determined from the combined data, Table 5.

Table 5 Flow calibration constants determined for each of the experimental configurations.

Calorimeter	***Flow Aligned*** ($\theta = \theta_{null} \pm 90°$)	***Axis Aligned*** ($\theta = 0°$)	***Ambient***	***NG Fire***	**All Data (mass flow range)**
3 MW	1.038	1.042	1.040	1.042	**1.040 ± 0.075** (13 kg/s to 28 kg/s)
10 MW	1.050	1.052	1.052	1.046	**1.051 ± 0.071** (27 kg/s to 56 kg/s)
20 MW	1.037	1.057	1.049	1.072	**1.049 ± 0.065** (53 kg/s to 116 kg/s)

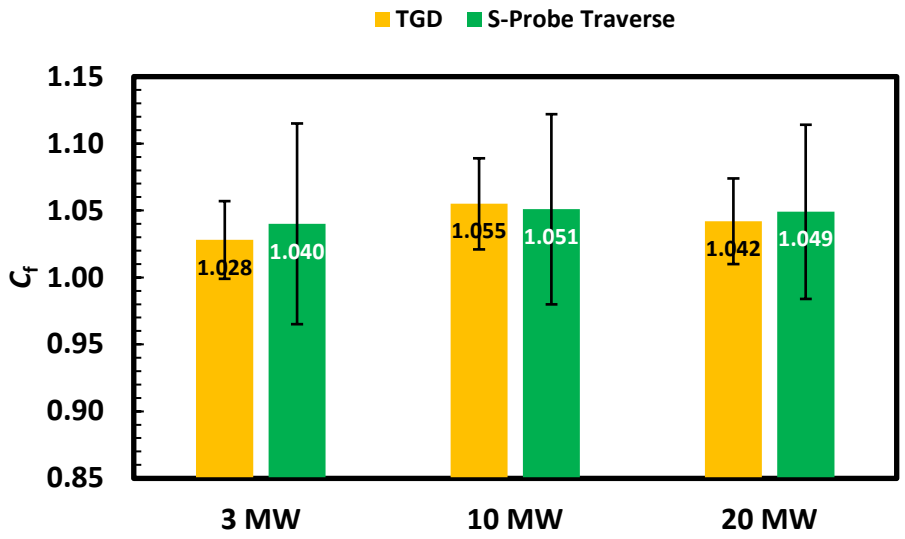

Fig. 15. Comparison of flow calibration constants determined using independent calibration techniques, tracer gas dilution (TGD) and pitot (S-Probe) traverse. Error bars represent estimates of expanded uncertainty.

The flow calibration constants determined here agree with those determined for previous in-line calibration experiments using tracer gas dilution as the reference flow measurement. [17, 18, 24] The difference between the calibration constants is ±0.01 or less, which is less than the standard uncertainty of either calibration method, therefore confirming equivalent results. Heated flow conditions are included in the present study, unlike the previous calibration using tracer gas dilution. Depending on the calorimeter and therefore the flow path, the addition of a fire potentially impacts the flow calibration, as observed at the 20 MW calorimeter. The present results provide more evidence that flow calibrations for ambient conditions are applicable for the full range of operating conditions of NFRL's 3 MW and 10 MW calorimeters. This study completes the goal of conducting in-line calibrations of NFRL's averaging pitot probes using two independent techniques as reference flow measurements. Frequent flow calibrations using the tracer gas dilution method with sulfur hexafluoride (SF_6) as the tracer are not recommended as SF_6 is a potent greenhouse gas. The agreement in calibration results demonstrate that future calibrations using the S-probe traverse will be adequate.

5. Summary

Accurate measurements of heat release rate using oxygen consumption calorimetry require accurate measurements of the exhaust flow. Averaging pitot probes have been installed in the exhaust ducts of the NFRL to provide continuous measurements of exhaust flow during large fire experiments. The devices are commercially available and widely used to monitor flows for industrial processes, but their accuracy depends on the flow distribution for their installation. A detailed characterization of exhaust flow for NFRL's calorimetry measurement system has been conducted to improve the accuracy its averaging pitot probes.

Experiments were conducted using S-probes to measure the flow distribution on two orthogonal chords of the exhaust ducts. The experiments followed the fundamental procedures of several standard methods for determining average flow in exhaust ducts and stacks (EPA Method 2, EPA Method 2G, ASTM D3154, and ISO 10780). The results characterize the distribution of near-axial velocity, flow angle, and gas temperature at each of the exhaust ducts. Flow angles were less than 15° on average. Therefore, it is practical to align the S-probes with the duct axis when conducting flow traverse experiments in NFRL's exhaust ducts and achieve sufficient accuracy. The addition of a fire did not alter the flow distribution or impact the flow calibration constant for the 3 MW and 10 MW calorimeters. Therefore, experiments with ambient flow are sufficient to characterize each of these calorimeters. The addition of fire at the 20 MW calorimeter has potential to alter the flow distribution enough to impact the flow calibration constant. Due to the limited data the evidence is inconclusive, and more experiments are necessary to fully characterize the impact of a fire at the 20 MW calorimeter. Temperature measurements were also conducted as part of the profiling experiments. The results show that gas temperature is uniformly distributed across the exhaust ducts. Hence the temperature measurement at the averaging pitot probe serves as a good estimate of average temperature at the exhaust flow.

The experiments spanned the range of routine operating conditions of NFRL's exhaust ducts. Repeatable results were observed over a period of 24 months, indicating that the flow conditions remain stable. Polynomial fits were generated from the data to compute estimates of the relative flow distribution, $V_{est}(d)/V_{APP}$, along the horizontal and vertical chords. This provides a tool for future investigations, such as simulations of fire experiments or sampling campaigns of smoke and particulate emissions. For a given flow speed at the averaging pitot probes, the estimated local exhaust flow, $V_{est}(d)$, can be used to tune particulate sampling equipment to achieve iso-kinetic flow for improved accuracy. The experimental results also provide high fidelity data that may be applied to tune or validate computational models, such as the Fire Dynamics Simulator, when used to simulate fire experiments conducted in the NFRL for other than routine conditions.

Average exhaust velocity computed from the flow distributions serve as reference measurements for in-line calibrations of continuous flow monitoring devices. The present study completes the goal of conducting in-line calibrations of NFRL's averaging pitot probes using two independent reference measurements, a volume flow measurement using tracer gas dilution and an average flow velocity measurement using S-probes. Both methods, as applied, are traceable to NIST primary flow standards. The flow calibration constants determined by the

two methods agree within 1 %, which is less than their respective standard uncertainty and thereby confirms the accuracy of the two methods, as applied, and the accuracy of the flow calibration. Uncertainty estimates for the calibration using the S-probe traverse range from 6 % to 7 %. This is a factor of two greater than uncertainty estimates for the calibration with tracer gas dilution, but the agreement in calibration results provide evidence that future calibrations using the S-probe traverse will provide adequate traceability to the initial calibration.

This effort has established a benchmark for the accuracy of the NFRL's exhaust flow measurement as well as established a reference for the distribution of flow in the three large exhaust ducts for NFRL's 20 MW calorimetry measurement system. The data presented here will be useful to evaluate the impact of future physical or operational changes to the system as well as evaluating its stability over time. This effort has also provided additional evidence that in-situ calibration of the flow monitoring devices used for large fire calorimetry is best practice. Procedures for the flow calibration exist as consensus standards, developed by the industry for monitoring emissions due to fossil fuel combustion at stationary sources. These procedures were applied for the NFRL and can be applied for similar fire test facilities to improve the accuracy of their large fire calorimetry measurements.

References

[1] Bryant RA , Bundy MF (2019) The NIST 20 MW Calorimetry Measurement System for Large-Fire Research. (National Institute of Standards and Technology, Gaithersburg, MD), NIST TN 2077. https://doi.org/10.6028/NIST.TN.2077

[2] Janssens ML (2002) Calorimetry. *The SFPE Handbook of Fire Protection Engineering*, ed DiNenno PD, D; Beyler, CL; Walton, WD; Custer, RLP; Hall, JR; Watts, JM (National Fire Protection Association, Quincy, MA), Chapter 2, 3rd Ed., pp Section 3:38-62.

[3] Yeager RW (1986) Uncertainty Analysis of Energy-Release Rate Measurement for Room Fires. *Journal of Fire Sciences* 4(4):276-296. https://doi.org/10.1177/073490418600400404

[4] Enright PA , Fleischmann CM (1999) Uncertainty of heat release rate calculation of the ISO5660-1 cone calorimeter standard test method. *Fire Technology* 35(2):153-169. https://doi.org/10.1023/A:1015416005888

[5] Axelsson J, Andersson P, Lonnermark A, VanHees P, Wetterlund I (2001) Uncertainties in Measuring Heat and Smoke Release Rates in the Room/Corner Test and the SBI. (Boras, Sweden), SP Report 2001:04, 2001.

[6] Brohez S (2005) Uncertainty analysis of heat release rate measurement from oxygen consumption calorimetry. *Fire and Materials* 29(6):383-394. https://doi.org/10.1002/fam.895

[7] Sette B (2005) Evaluation of Uncertainty and Improvement of the Single Burning Item Test Method. (Ph.D. Thesis, University of Ghent, Belgium).

[8] Bryant RA , Mulholland GW (2008) A guide to characterizing heat release rate measurement uncertainty for full-scale fire tests. *Fire and Materials* 32(3):121-139. https://doi.org/10.1002/fam.959

[9] ASTM (2015) Standard Practice for Full-Scale Oxygen Consumption Calorimetry Fire Tests. (ASTM International, West Conshohocken, PA), ASTM E 2067-15.

[10] ISO (2008) Fire Tests - Open Calorimetry - Measurement of the Rate of Production of Heat and Combustion Products for Fires of up to 40 MW. (International Organization for Standardization, Switzerland), ISO 24473:2008(E).

[11] ASTM (2016) Standard Test Method for Heat and Visible Smoke Release Rates for Materials and Products Using an Oxygen Consumption Calorimeter. (ASTM International, West Conshohocken, PA), ASTM E 1354-16a.

[12] ASTM (2017) Standard Test Method for Room Fire Test of Wall and Ceiling Materials and Assemblies. (ASTM International, West Conshohocken, PA), ASTM E 2257-17.

[13] EPA (2007) Determination of Stack Gas Velocity and Volumetric Flow Rate with Two-Dimensional Probes. (Environmental Protection Agency, Washington, D.C.), EPA Method 2G, February 2007.

[14] ASTM International (2006) Standard Test Method for Average Velocity in a Duct (Pitot Tube Method). ASTM D3154-00, May 2006.

[15] ISO (1994) Stationary Source Emissions - Measurement of Velocity and Volume Flowrate of Gas Streams in Ducts. (International Organization for Standardization, Switzerland), ISO 10780:1994(E).

[16] Bryant RA , Bundy MF (2021) Improving the State-of-the-Art in Flow Measurements for Large-Scale Oxygen Consumption Calorimetry. *Fire Technol* 57(3):22. https://doi.org/10.1007/s10694-020-01066-x

[17] Bryant RA (2022) The NIST 20 MW Calorimetry Measurement System - Exhaust Flow Calibration Using Tracer Gas Dilution. (National Institute of Standards and Technology, Gaithersburg, MD), NIST TN 2220. https://doi.org/10.6028/NIST.TN.2220

[18] Bryant RA (2024) Exhaust flow calibration for a large-scale calorimetry system using tracer gas dilution. *Fire and Materials* 48(2):286-296. https://doi.org/10.1002/fam.3183

[19] EPA (2000) Sample and Velocity Traverses for Stationary Sources. (Environmental Protection Agency, Washington, D.C.), EPA Method 1, February 2000.

[20] EPA (2000) Determination of Stack Gas Velocity and Volumetric Flow Rate (Type S Pitot Tube). (Environmental Protection Agency, Washington, D.C.), EPA Method 2, February 2000.

[21] Bryant RA, Chernovsky, A. A., Falco J. A., Shinder, I. I. (2023) An Automated System for Flow Characterization at Exhaust Ducts and Smokestacks. (National Institute of Standards and Technology, Gaithersburg, MD). https://doi.org/10.6028/NIST.TN.2247

[22] Shinder II, Moldover MR, Filla BJ, Johnson AN, Khromchenko VB (2021) Facility for calibrating anemometers as a function of air velocity vector and turbulence. *Metrologia* 58(4). https://doi.org/10.1088/1681-7575/ac0a92

[23] Shinder II, Crowley CJ, Filla BJ, Moldover MR (2015) Improvements to NIST'S air speed calibration service. *Flow Measurement and Instrumentation* 44:19-26. https://doi.org/10.1016/j.flowmeasinst.2014.11.005

[24] Bryant RA (2018) Uncertainty estimates of tracer gas dilution flow measurements in large-scale exhaust ducts. *Flow Meas Instrum* 61:1-8. https://doi.org/10.1016/j.flowmeasinst.2018.03.004

[25] ISO (2008) Evaluation of Measurement Data - Guide to the Expression of Uncertainty in Measurement. (International Organization for Standardization, Switzerland), JCGM 100:2008.

Appendix A. List of Symbols

$\boldsymbol{C}$
calibration constant

$\boldsymbol{D}$
inner diameter of exhaust duct or smokestack

$\boldsymbol{d}$
traverse position across the exhaust duct or smokestack

$\Delta_{\mathbf{c}}\boldsymbol{H}$

net heat of combustion; lower heating value (LHV)

$\boldsymbol{k}$

coverage factor

$\dot{\boldsymbol{m}}$

mass flow

$\boldsymbol{M}$
molecular mass or number of repeat experiments

$\boldsymbol{N}$
number of centroid of equal area measurement locations

$\boldsymbol{P}$
pressure

$\Delta\boldsymbol{P}$
differential pressure

$\dot{\boldsymbol{Q}}$

heat release rate

$\boldsymbol{R}$

universal gas constant

$\boldsymbol{s}$

non dimensional sensitivity coefficient

$\boldsymbol{T}$
temperature

$\boldsymbol{u}$
standard uncertainty

$\boldsymbol{U}$
expanded uncertainty (95 % confidence interval, k = 2.0)

$\boldsymbol{V}$
gas velocity

$\boldsymbol{x}$

input quantity for measurement model

$\boldsymbol{y}$

output quantity of measurement model

Greek

ρ
gas density

σ
standard deviation (repeatability)

θ
rotational position of probe (angle relative to axis of exhaust duct or smokestack)

Subscripts

APP
averaging pitot probe

CEA
centroid of equal area

e
exhaust

f
flow measurement

OC
oxygen consumption

s
static

SP
S-probe

Appendix B. Flow Traverse Positions

Table B.1 CEA traverse positions, d_i/D, for circular ducts.

Traverse Point, i	6 Points on Diameter	12 Points on Diameter	24 Points on Diameter
1	0.044	0.021	0.011
2	0.146	0.067	0.032
3	0.296	0.118	0.055
4	0.704	0.177	0.079
5	0.854	0.250	0.105
6	0.956	0.356	0.132
7		0.644	0.161
8		0.750	0.194
9		0.823	0.230
10		0.882	0.272
11		0.933	0.323
12		0.979	0.398
13			0.602
14			0.677
15			0.728
16			0.770
17			0.806
18			0.839
19			0.868
20			0.895
21			0.921
22			0.945
23			0.968
24			0.989

Appendix C. Uncertainty Estimate for Near-Axial Velocity Measurement

Estimates of measurement uncertainty were evaluated using the approximate methods described in the ISO GUM. [25] Measurement processes that were based on input measurements, x_i, were modeled as an output quantity, y:

$$y = y(x_1, x_2, x_3, \ldots, x_N) \quad \text{(C1)}$$

In the case that all input quantities, x_i, are uncorrelated, the relative combined standard uncertainty is given by

$$\frac{u(y)}{y} = \sqrt{\sum_{i=1}^{N} \left(s_i \frac{u(x_i)}{x_i} \right)^2} \quad \text{(C2)}$$

Where $u(x_i)$ is the standard uncertainty for each input, and s_i is the associated dimensionless sensitivity coefficient given by

$$s_i = \frac{\partial y}{\partial x_i} \frac{x_i}{y} \quad \text{(C3)}$$

Equation (C2) provides the propagation of uncertainty from each instrument and input parameter into the measurement model, Eq. (C1). The relative expanded uncertainty is defined as:

$$\frac{U(y)}{y} = k \frac{u(y)}{y} \quad \text{(C4)}$$

Where k = 2.0, is the coverage factor for the 95 % confidence interval.

Table C.1 Estimated uncertainty budget for a near-axial velocity measurement, Eq. (4).

Measurement / Parameter, x_i	Value	$u(x_i)/x_i$	s_i	% Contribution
C_{SP} (-)	0.825	0.026*	1.0	98.0
θ (°)	1.8	0.880	-0.001	0.1
ΔP (Pa)	56.0	0.005	0.5	0.9
T (K)	290.7	0.005	0.5	0.9
P_s (Pa)	98 468	0.000 2	-0.5	0.0
M_e (kg /kmol)	28.97	0.0017	-0.5	0.1
R (J/kmol K)	8314.47	0.000 0	0.5	0.0
$V_{SP,i}(d)$ (m/s)	**8.04**	**0.0267**	**Standard, $u(y)/y$**	
		0.053	**Expanded, $U(y)/y$**	

*Includes uncertainty contribution for probe misalignment within ±5°.

Whenever the mean value for a sample of measurements is reported, the uncertainty of the mean, also known as the standard deviation of the mean, $\frac{\sigma}{\sqrt{N}}$, contributes to the uncertainty of the reported value. For the present study, the S-probe held each position for a minimum of 30 s; acquiring velocity readings at a sample rate of 1 Hz. The mean velocities, $V_{\mathrm{SP}}(d)$ and $V_{\mathrm{APP}}(d)$, for 30 samples are logged. Flow speed was relatively steady for the duration of an experiment, with fluctuations due to turbulence. The mean ratio, $V_{\mathrm{SP}}(d)/V_{\mathrm{APP}}(d)$, is analyzed and reported to provide well established reference conditions for comparisons. For the present case the standard deviation of the mean represents the error of the measurement due to the turbulent nature of the flow. The relative standard deviation of the mean (SDOM) ranged from 0.002 to 0.023. Table C.1 demonstrates an uncertainty budget for a single sample, i, of velocity. This relative standard uncertainty is 0.028 on average. The uncertainty for the reported value, therefore the mean velocity at position *d*, is the combined uncertainty due to the measurement and the variation of the observed process (flow fluctuations). Computing the square root of the sum of squares of the relative standard uncertainty and the relative standard deviation of the mean, the estimated relative standard uncertainty for $V_{\mathrm{SP}}(d)$ is 0.030 on average with a range of 0.019 to 0.038.

Table C.2 Estimated combined uncertainty for reported values of near-axial velocity.

	Minimum	Maximum	Average
$u_{V_{\mathrm{SP}}(d)}/V_{\mathrm{APP}}(d)$	0.018	0.034	0.028
$\frac{\sigma/\sqrt{N}}{V_{\mathrm{APP}}(d)}$	0.002	0.023	0.008
$\sqrt{\left(\frac{u_{V_{\mathrm{SP}}(d)}}{V_{\mathrm{APP}}(d)}\right)^2+\left(\frac{\sigma/\sqrt{N}}{V_{\mathrm{APP}}(d)}\right)^2}$	0.019	0.038	**0.030 (Standard)**
	0.038	0.076	**0.060 (Expanded)**

Appendix D. Flow Distributions

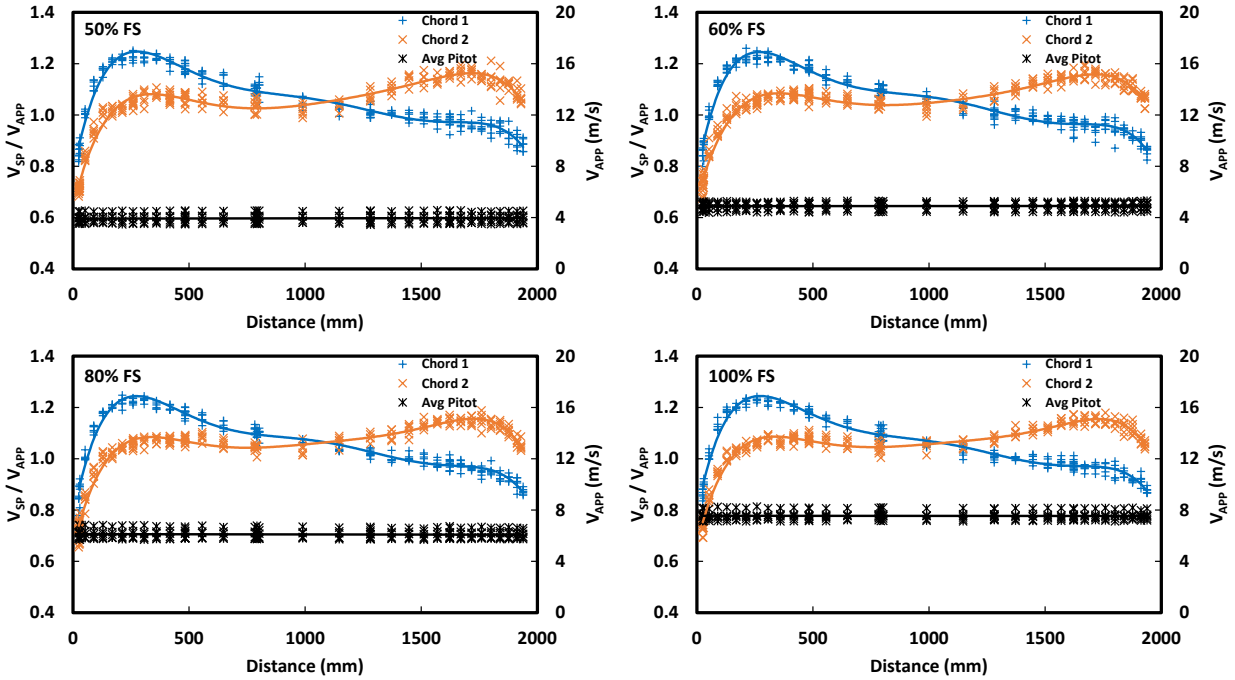

Fig. D.1. Flow distribution across the exhaust duct for the 3 MW calorimeter. Traverses were at the horizontal (1) and vertical (2) chords. Velocity measurements from the S-probes, V_{SP}, are plotted on the left axis and normalized by the corresponding flow monitored at the averaging pitot probes, V_{APP}. Measurements at the averaging pitot probes are plotted on the right axis for settings at 50 %, 60 %, 80 %, and 100 % of the calorimeter's mass flow capacity (Table 1).

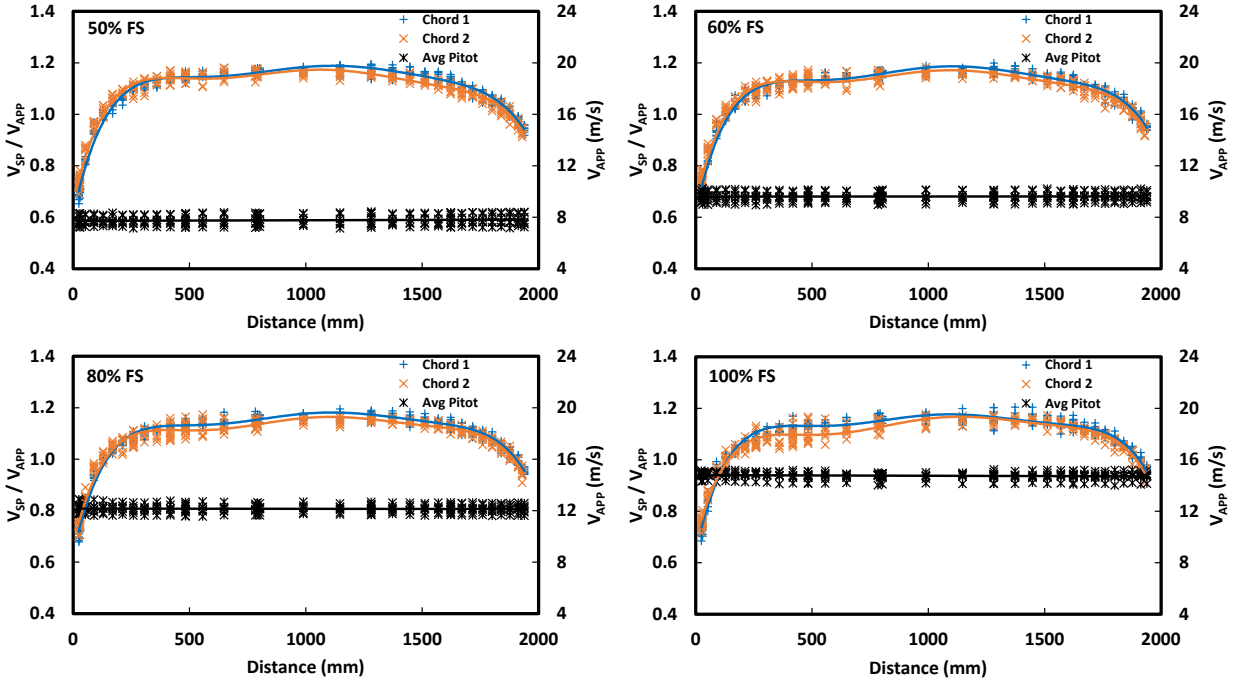

Fig. D.2. Flow distribution across the exhaust duct for the 10 MW calorimeter. Traverses were at the horizontal (1) and vertical (2) chords. Velocity measurements from the S-probes, V_{SP}, are plotted on the left axis and normalized by the corresponding flow monitored at the averaging pitot probes, V_{APP}. Measurements at the averaging pitot probes are plotted on the right axis for settings at 50 %, 60 %, 80 %, and 100 % of the calorimeter's mass flow capacity (Table 1).

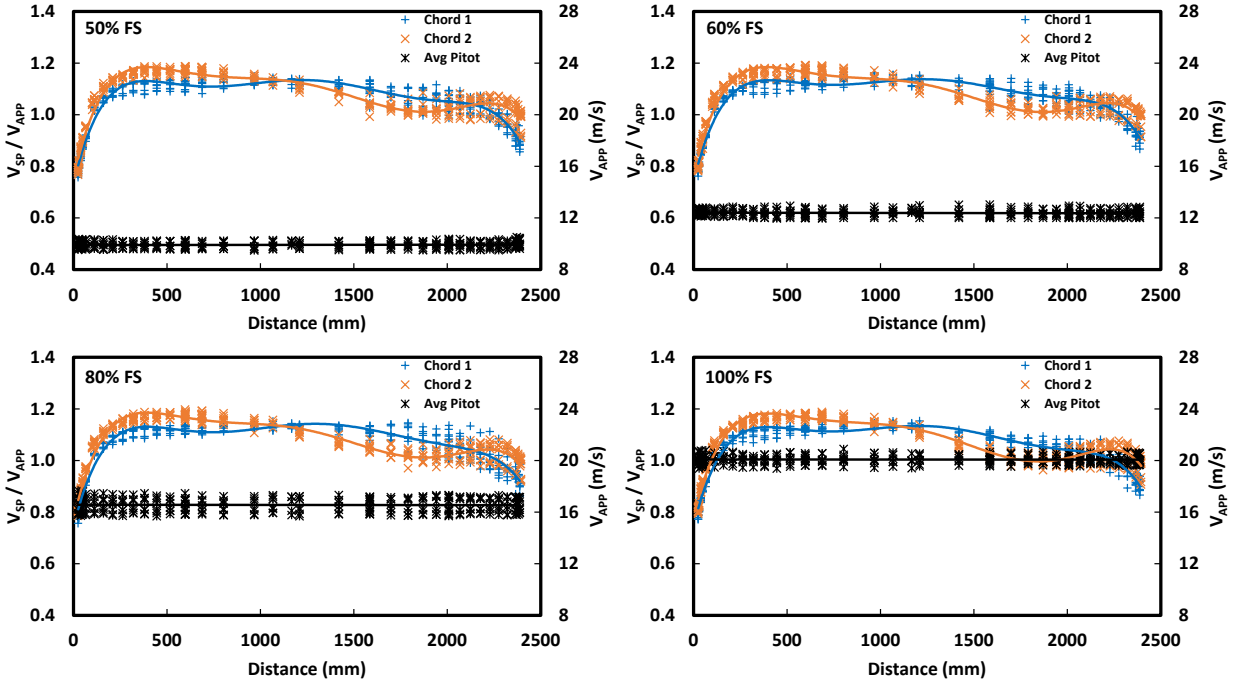

Fig. D.3. Flow distribution across the exhaust duct for the 20 MW calorimeter. Traverses were at the horizontal (1) and vertical (2) chords. Velocity measurements from the S-probes, V_{SP}, are plotted on the left axis and normalized by the corresponding flow monitored at the averaging pitot probes, V_{APP}. Measurements at the averaging pitot probes are plotted on the right axis for settings at 50 %, 60 %, 80 %, and 100 % of the calorimeter's mass flow capacity (Table 1).

Appendix E. Flow Distributions – Data from Polynomial Fits

Normalizing the velocity traverse measurements by measurements at the averaging pitot probe, collapsed the data on each chord into a single profile for the full range of flow conditions. Hence, a linear regression analysis with the least squares approach was conducted to compute velocity profiles at each calorimeter. A sixth-degree polynomial was chosen to fit the collapsed data, Eq. (E1). Using Table E.1, estimates of flow velocity, $V_{est}(d)$, at any position within the given range along the horizontal and vertical chord can be computed with knowledge of the uncorrected velocity measurement at the averaging pitot probes, V_{APP}. Calculated values of $V_{\mathrm{est}}(d)/V_{\mathrm{APP}}$ for 24 CEA locations are listed in Table E.2.

$$\frac{V_{\mathrm{est}}(d)}{V_{\mathrm{APP}}} = c_6 d^6 + c_5 d^5 + c_4 d^4 + c_3 d^3 + c_2 d^2 + c_1 d + c_0 \qquad \text{(E1)}$$

Table E.1 Coefficients for polynomial fits to estimate the distribution of flow velocity, Eq. (E1).

c_i	3 MW (25 mm ≤ d ≤ 1911 mm)		10 MW (25 mm ≤ d ≤ 1911 mm)		20 MW (26 mm ≤ d ≤ 2346 mm)	
	Hrztl	Vrtcl	Hrztl	Vrtcl	Hrztl	Vrtcl
c_0	7.7849E-01	6.5710E-01	6.2947E-01	6.6740E-01	7.4138E-01	7.6911E-01
c_1	4.6254E-03	3.6387E-03	4.0132E-03	3.8192E-03	2.9468E-03	3.1288E-03
c_2	-1.6306E-05	-1.1508E-05	-1.2524E-05	-1.2435E-05	-8.3288E-06	-8.8218E-06
c_3	2.5644E-08	1.7224E-08	1.9379E-08	1.9774E-08	1.1137E-08	1.1844E-08
c_4	-2.0561E-11	-1.3455E-11	-1.5532E-11	-1.6131E-11	-7.5582E-12	-8.2072E-12
c_5	8.1615E-15	5.3462E-15	6.1843E-15	6.5005E-15	2.5127E-15	2.7955E-15
c_6	-1.2715E-18	-8.5237E-19	-9.7100E-19	-1.0290E-18	-3.2558E-19	-3.6903E-19

Table E.2 Relative flow distribution, calculated at 24 CEA locations.

3 MW Calorimeter $\frac{V_{\text{est}}(d)}{V_{\text{APP}}}$			10 MW Calorimeter $\frac{V_{\text{est}}(d)}{V_{\text{APP}}}$			20 MW Calorimeter $\frac{V_{\text{est}}(d)}{V_{\text{APP}}}$		
d **(mm)**	**Hrztl**	**Vrtcl**	***d*** **(mm)**	**Hrztl**	**Vrtcl**	***d*** **(mm)**	**Hrztl**	**Vrtcl**
25	0.884	0.741	**25**	0.722	0.755	**26**	0.811	0.843
64	1.013	0.847	**64**	0.839	0.865	**78**	0.926	0.965
109	1.119	0.937	**109**	0.941	0.959	**134**	1.011	1.055
156	1.190	1.003	**156**	1.016	1.027	**192**	1.069	1.118
207	1.230	1.047	**207**	1.069	1.073	**254**	1.106	1.157
261	1.245	1.073	**261**	1.103	1.101	**320**	1.125	1.178
319	1.240	1.083	**319**	1.123	1.116	**391**	1.131	1.184
383	1.220	1.082	**383**	1.132	1.120	**470**	1.128	1.180
454	1.190	1.073	**454**	1.134	1.120	**557**	1.121	1.170
537	1.156	1.059	**537**	1.135	1.119	**659**	1.114	1.159
638	1.122	1.046	**638**	1.140	1.123	**783**	1.112	1.149
786	1.094	1.039	**786**	1.155	1.140	**965**	1.123	1.141
1189	1.040	1.071	**1189**	1.180	1.168	**1459**	1.123	1.072
1337	1.008	1.093	**1337**	1.167	1.154	**1641**	1.097	1.031
1438	0.988	1.112	**1438**	1.154	1.141	**1765**	1.078	1.011
1521	0.978	1.131	**1521**	1.143	1.131	**1867**	1.066	1.006
1592	0.973	1.146	**1592**	1.133	1.123	**1954**	1.058	1.009
1656	0.971	1.158	**1656**	1.122	1.114	**2033**	1.051	1.019
1714	0.969	1.164	**1714**	1.109	1.102	**2104**	1.044	1.030
1768	0.964	1.162	**1768**	1.091	1.085	**2170**	1.033	1.038
1819	0.953	1.149	**1819**	1.065	1.060	**2232**	1.015	1.041
1866	0.933	1.124	**1866**	1.030	1.025	**2290**	0.988	1.034
1911	0.900	1.084	**1911**	0.984	0.978	**2346**	0.949	1.013
1950*	0.603	0.585	***1950***	0.660	0.524	***2398***	0.644	0.853

*Linear interpolation between far wall ($V(D) = 0$) and limit of polynomial fit.